Annals of Nuclear Energy 85 (2015) 937–957

Contents lists available at ScienceDirect

Annals of Nuclear Energy

journal homepage: www.elsevier.com/locate/anucene

A nonoverlapping local/global iterative method with 2-D/1-D fusion transport kernel and p-CMFD wrapper for transient reactor analysis

Bumhee Cho, Nam Zin Cho *

Department of Nuclear and Quantum Engineering, Korea Advanced Institute of Science and Technology, 291 Daehak-ro, Yuseong-gu, Daejeon 305-701, Republic of Korea

ARTICLE INFO

Article history:
Received 24 November 2014
Received in revised form 15 June 2015
Accepted 1 July 2015
Available online 26 July 2015

Keywords:
Nonoverlapping local/global (NLG) iteration
2-D/1-D fusion method
p-CMFD
3-D transient transport
Rod cusping
Neighboring spectral index (NSI) weighting method

ABSTRACT

As modern computing power grows, whole-core transport calculations become more viable. However, the computing time and memory requirement remain major burdens. As a candidate for whole-core transport calculation methods, nonoverlapping local/global (NLG) iteration has recently been developed.

In this study, the NLG iteration method is extended to make it capable of transient calculations of 3-D heterogeneous problems. It is then implemented in an in-house code, CRX-2K. Transient NLG iteration uses the 2-D/1-D fusion method as a local transport kernel, with the transient p-CMFD equation adopted as a global wrapper. In addition, a neighboring spectral index (NSI) weighting method is suggested as a tool for correcting the rod cusping phenomenon for rod ejection problems.

Four problems, including a 3-D heterogeneous problem, are computed. Numerical results show that the NLG iteration converges to the reference solution obtained by means of the whole-core p-CMFD acceleration, and the NSI weighting method is accurate to correct the rod cusping phenomenon. The NLG iteration in present implementation takes more computing times (still less than 2 times) than the whole-core p-CMFD acceleration, but has great potential in parallelization.

1. Introduction

In conventional reactor core analyses, multi-group diffusion nodal methods are used, and corresponding nodal parameters are obtained by isolated single-assembly transport calculations under all-reflective boundary condition. Single-assembly calculations do not reflect the inter-assembly transport effects (i.e., flux gradients) which arise when these types of assemblies are loaded into a real reactor core. Hence, the nodal parameters obtained by single-assembly calculations do not properly incorporate the transport effects, leading to inaccurate solutions compared to whole-core transport solutions.

As modern computing power grows, direct whole-core transport calculations become more viable. However, these are not fully feasible yet as a practical reactor core analysis tool due to the huge computational burden they incur (Smith et al., 2003; Hoogenboom et al., 2010) in terms of both the computing time and memory requirements. To reduce the computing time required during a whole-core transport calculation, acceleration methods using low-order equations have been developed. For example, the coarse-mesh finite difference (CMFD) method (Smith and Rhodes, 2000) is an efficient acceleration tool, but it has divergence issues in optically thick regions. As an alternative to the CMFD method, the partial-current-based coarse-mesh finite difference (p-CMFD) method has been developed. It shows more stable convergence than CMFD, as shown in Fourier analysis and numerical tests (Cho et al., 2003; Cho, 2012).

In this era, increased computing power by increasing the CPU clock speed is limited, but computing power is growing through the adoption of parallel hardware architectures (Sutter, 2005). Hence, whole-core transport calculations would be more efficient if parallel calculations are adopted. For this purpose, local/global iterative methods are suitable considering that the main feature of local/global iterative methods is that the local problems are independent of each other. Moreover, heavy calculation burdens are usually caused by local transport calculations, implying that the parallel computing of local problems will reduce the calculation time and lessen the computing memory requirements. For example, the boundary condition perturbation theory (Rahnema, 1989; Kim and Cho, 1993; Rahnema and McKinley, 2002), and tabulated nodal parameters for various albedo boundary conditions (Clarno and Adams, 2005) have been developed. There was also an attempt to apply a local/global iterative method to a direct 3-D method of characteristics (MOC) calculation (Kochunas, 2013) by means of spatial domain decomposition with CMFD (SDD-CMFD) (Kelley and Larsen, 2012).

* Corresponding author. Tel.: +82 (42) 350 3819; fax: +82 (42) 350 3810.
E-mail address: nzcho@kaist.ac.kr (N.Z. Cho).

http://dx.doi.org/10.1016/j.anucene.2015.07.012
0306-4549/

As an independent area of research, an overlapping local/global (OLG) iteration method (in short, the OLG iteration) has been proposed (Cho et al., 2013). OLG iteration consists of a two-level iterative approach in which half-assembly overlapping local problems are solved by a transport solver, with these local problems coupled by a global wrapper of the p-CMFD equation. The local problems are tightly coupled, as the local domains are overlapped onto each other. Despite this advantage, the computation time is much longer (at least doubled) compared to the whole-core p-CMFD acceleration due to the increased total computing domain (Yuk et al., 2013; Yoo et al., 2015).

As an alternative to OLG iteration, the nonoverlapping local/-global (NLG) iterative method (in short, the NLG iteration) has been developed (Yuk and Cho, 2014). NLG iteration is also a two-level iterative approach, but the local domains do not overlap. Therefore, the total local domain size is identical to the original problem domain size. Though the local problems in this case are entirely independent of each other, the inter-assembly transport effects are nonetheless well reflected by the global wrapper of the p-CMFD equation. Moreover, the p-CMFD equation provides transport partial currents at the local domain boundaries. NLG iteration was successfully applied to steady-state 3-D heterogeneous transport problems with the 2-D/1-D fusion method (Cho et al., 2002, 2003) as a local kernel, showing that the NLG iteration method converges to a solution identical to that gained when using whole-core p-CMFD acceleration with reasonable computing time (Yuk and Cho, 2014).

In recent years, several groups have paid attention to the development of codes to solve the 3-D time-dependent neutron transport equation such as Variant-K (Rineiski and Doriath, 1997), DeCART (Joo et al., 2004), TORT-TD (Seubert et al., 2008), and MOCK-3DK (Taylor and Baratta, 2009). TORT-TD is based on S_N method, so heterogeneous geometry cannot be treated explicitly. MOCK-3DK is based on the 3-D MOC method, but a 3-D application is not feasible yet due to exorbitant computation burden and the absence of an accelerator (Taylor and Baratta, 2009). Variant-K is based on the variational nodal method (Rineiski and Doriath, 1997), and this code basically requires cell or assembly-wise homogenized cross sections. DeCART is based on 2-D/1-D "hybrid" method, and the 2-D calculation is carried out by the MOC method which deals heterogeneous geometry in the radial direction explicitly. However, the 1-D solution is approximated by a diffusion solution in a homogenized cell level. Therefore, axial leakage source terms (or axial transverse leakages, TL) for the 2-D calculation are limited by diffusion approximation in a homogenized cell level. All of the codes transform the time-dependent neutron transport equation into the form of steady-state equation, so called a transient fixed source problem (TFSP).

In this paper, the NLG iteration method is extended to make it capable of transient calculations for 3-D heterogeneous problems. Both the local kernel of 2-D/1-D fusion method and the global wrapper of p-CMFD acceleration are extended to transient calculations. This paper is organized as follows. In Section 2, the transient 2-D/1-D fusion method is derived from a time-dependent neutron transport equation to have the TFSP. In Section 3, the transient p-CMFD equation is derived from the discretized transport equation obtained in Section 2. In Section 4, NLG iteration is described with the transient 2-D/1-D fusion method as the local kernel and the transient p-CMFD equation as the global wrapper. Numerical results are shown in Section 5, and conclusions are presented in Section 6.

2. Transient 2-D/1-D fusion method

As a candidate for a heterogeneous 3-D transport solver, the 2-D/1-D fusion method was developed (Cho et al., 2002, 2003; Lee and Cho, 2006; Lee, 2006). The basic idea of this method is that a 3-D transport equation is decomposed into 2-D and 1-D equations by means of "consistent directional decomposition and integration". Fig. 1 shows a schematic illustration of the 2-D/1-D fusion method. A conventional nuclear reactor core is usually strongly heterogeneous in the radial direction, while it is piecewise homogeneous in the axial direction. Therefore, the MOC method is used to deal with the complicated geometry in the radial direction, and a S_N-like method is used in the axial direction. These 2-D and 1-D equations are coupled by axial and radial leakage source terms such that the 2-D/1-D fusion method would result in a 3-D transport solution via an iterative solution approach. However, the 2-D/1-D fusion method has been developed only for a steady-state calculation. In this section, the 2-D/1-D fusion method will be extended to transient calculations.

2.1. Time-dependent neutron transport equation

To formulate a time-discretized multi-group transport equation, we consider the following time-dependent neutron transport equation:

$$\frac{1}{v_g}\frac{\partial \psi_g(\vec{r},\vec{\Omega},t)}{\partial t}+\vec{\Omega}\cdot\nabla\psi_g(\vec{r},\vec{\Omega},t)+\sigma_{t,g}\psi_g(\vec{r},\vec{\Omega},t) = \frac{1}{4\pi}\left[\frac{(1-\beta)}{k_{eff}}\chi_g\sum_{g'}\nu\sigma_{f,g'}\phi_{g'}(\vec{r},t)+\sum_{g'}\sigma_{s0,g'\to g}\phi_{g'}(\vec{r},t) + \sum_d \chi_{d,g}\lambda_d C_d(\vec{r},t)\right]. \quad (1)$$

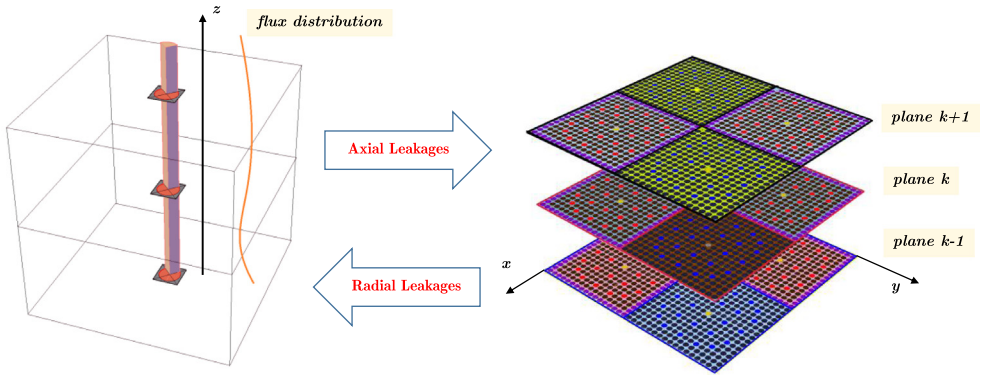

Fig. 1. Schematic illustration of 2-D/1-D fusion method.

Here, g is the fine-energy group index, d is the delayed neutron precursor family index, C_d is the delayed neutron precursor concentration of family d, and the other notations are standard. For the sake of brevity, space and time indices in other quantities such as cross sections are omitted, and only isotropic scattering is considered. k_{eff} and initial condition of flux are obtained by the steady-state NLG iteration, and the steady-state methodology is described elsewhere (Yuk and Cho, 2014).

Eq. (2) below represents the delayed neutron precursor concentration equation for family d:

$$\frac{\partial C_d(\vec{r},t)}{\partial t} = -\lambda_d C_d(\vec{r},t) + \frac{\beta_d}{k_{eff}} \sum_{g'=1} \nu\sigma_{f,g'}\phi_{g'}(\vec{r},t). \tag{2}$$

The fully implicit method is applied to the time derivative term in Eq. (1) at a time step of $n+1$, as follows:

$$\frac{1}{v_g}\frac{\partial \psi_g(\vec{r},\vec{\Omega},t_{n+1})}{\partial t} \approx \frac{1}{v_g}\frac{\psi_g(\vec{r},\vec{\Omega},t_{n+1}) - \psi_g(\vec{r},\vec{\Omega},t_n)}{\Delta t_{n+1}}, \tag{3}$$

where $\Delta t_{n+1} = t_{n+1} - t_n$.

In a practical application, Eq. (3) would incur massive memory requirements, as all angular fluxes in the complete problem domain of the previous time step must be saved. To avoid this issue, the angular dependency in Eq. (3) is assumed to be isotropic, as follows:

$$\frac{1}{v_g}\frac{\psi_g(\vec{r},\vec{\Omega},t_{n+1}) - \psi_g(\vec{r},\vec{\Omega},t_n)}{\Delta t_{n+1}} \approx \frac{1}{4\pi}\left[\frac{1}{v_g}\frac{\phi_g(\vec{r},t_{n+1}) - \phi_g(\vec{r},t_n)}{\Delta t_{n+1}}\right]. \tag{4}$$

Eq. (4) would have a negligible impact on the accuracy of the solution (Cho et al., 2005a; Talamo, 2013), as the assumption of isotropy is applied to the angular flux in the time difference term, not to the angular flux itself. By substituting Eq. (4) into Eq. (1), the following equation is obtained:

$$\begin{aligned}&\vec{\Omega}\cdot\nabla\psi_g(\vec{r},\vec{\Omega},t_{n+1}) + \sigma_{t,g}\psi_g(\vec{r},\vec{\Omega},t_{n+1})\\ &= \frac{1}{4\pi}\left[\frac{(1-\beta)}{k_{eff}}\chi_g\sum_{g'}\nu\sigma_{f,g'}\phi_{g'}(\vec{r},t_{n+1}) + \sum_{g'}\sigma_{s0,g'\to g}\phi_{g'}(\vec{r},t_{n+1})\right.\\ &\quad\left. + \sum_d \chi_{d,g}\lambda_d C_d(\vec{r},t_{n+1}) - \frac{1}{v_g}\frac{\phi_g(\vec{r},t_{n+1}) - \phi_g(\vec{r},t_n)}{\Delta t_{n+1}}\right].\end{aligned} \tag{5}$$

Once the delayed neutron precursor concentrations are known in Eq. (5), Eq. (5) can be solved using a steady-state transport solver with a modified source term. A second-order precursor integration technique (Joo et al., 1998) is used to eliminate the delayed neutron precursor concentration, which is unknown at the current time step ($C_m(t_{n+1})$) in Eq. (5). Following this technique, the fission source term in Eq. (2) is assumed to be a quadratic polynomial in the time step, after which Eq. (2) can be integrated analytically with respect to time. Therefore, the delayed neutron precursor concentration at the current time step is expressed in terms of that in the previous time step and the fission sources at three different time steps, as follows:

$$\begin{aligned}C_d(\vec{r},t_{n+1}) = \tau_d C_d(\vec{r},t_n) + \frac{\beta_d}{\lambda_d}(&\Omega_{d,n-1}F(\vec{r},t_{n-1})\\ &+ \Omega_{d,n}F(\vec{r},t_n) + \Omega_{d,n+1}F(\vec{r},t_{n+1})),\end{aligned} \tag{6}$$

where

$$\Omega_{d,n-1} = \frac{1}{\lambda_d\Delta t_n(\gamma+1)}\left[\frac{2\tilde{\tau}_d}{\lambda_d\Delta t_n} - \gamma(\tau_d+1)\right], \tag{6a}$$

$$\Omega_{d,n} = \frac{1}{\lambda_d\Delta t_n}\left[\tau_d + 1 + \frac{\tilde{\tau}_d}{\gamma}\left(1 - \frac{2}{\lambda_d\Delta t_n}\right)\right] - \tau_d, \tag{6b}$$

$$\Omega_{d,n+1} = 1 - \frac{2}{\lambda_d\Delta t_n(\gamma+1)} + \frac{\tilde{\tau}_d}{\lambda_d\Delta t_n(\gamma+1)\gamma}\left(\frac{2}{\lambda_d\Delta t_n} - 1\right), \tag{6c}$$

$$\tau_d = e^{-\lambda_d\Delta t_{n+1}}, \tag{6d}$$

$$\tilde{\tau}_d = 1 - \tau_d, \tag{6e}$$

$$\gamma = \Delta t_{n+1}/\Delta t_n, \tag{6f}$$

$$F(\vec{r},t_n) = \frac{1}{k_{eff}}\sum_{g'}\nu\sigma_{f,g'}\phi_{g'}(\vec{r},t_n). \tag{6g}$$

By substituting Eq. (6) into Eq. (5), the time-discretized neutron transport equation is obtained as follows:

$$\vec{\Omega}\cdot\nabla\psi_g(\vec{r},\vec{\Omega},t_{n+1}) + \sigma_{t,g}\psi_g(\vec{r},\vec{\Omega},t_{n+1}) = \frac{1}{4\pi}q_g(\vec{r},t_{n-1},t_n,t_{n+1}), \tag{7}$$

where

$$\begin{aligned}&q_g(\vec{r},t_{n-1},t_n,t_{n+1})\\ &= \left[(\alpha_g + (1-\beta)\chi_g)F(\vec{r},t_{n+1}) + \sum_{g'=1}\sigma_{s0,g'\to g}\phi_{g'}(\vec{r},t_{n+1})\right.\\ &\quad\left. + S_g(\vec{r},t_n) - \frac{1}{v_g}\frac{\phi_g(\vec{r},t_{n+1}) - \phi_g(\vec{r},t_n)}{\Delta t_{n+1}}\right],\end{aligned} \tag{7a}$$

$$\alpha_g = \sum_d \chi_{d,g}\beta_d\Omega_{d,n+1}, \tag{7b}$$

$$S_g(\vec{r},t_n) = \sum_d \chi_{d,g}\tau_d\lambda_d C_d(\vec{r},t_n) + \sum_{l=n-1}^{n}\sum_d \chi_{d,g}\beta_d\Omega_{d,l}F(\vec{r},t_l). \tag{7c}$$

After Eq. (7) is discretized with regard to the angle, the angle-discretized equation in the direction of $\vec{\Omega}_j$ can be written in the ray plane coordinate illustrated in Fig. 2, as follows:

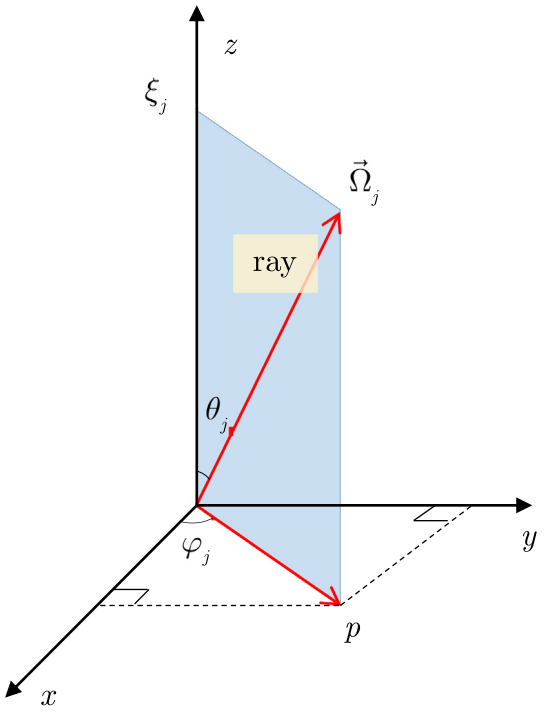

Fig. 2. Ray plane coordinates.

$$\sin\theta_j \frac{\partial \psi_{g,j}(p,z)}{\partial p} + \xi_j \frac{\partial \psi_{g,j}(p,z)}{\partial z} + \sigma_{t,g}\psi_{g,j}(p,z) = q_g(p,z), \tag{8}$$

where

$$\int_{4\pi} \psi_g(p,z,\vec{\Omega})d\Omega \simeq \sum_j \psi_{g,j}(p,z)w_j, \tag{8a}$$

$$\sum_j w_j = 4\pi. \tag{8b}$$

The time step index is omitted for the sake of brevity. In this study, the azimuthal angle set is chosen according to the product quadrature set (Lewis and Miller, 1984), which easily enables modular ray tracing (Filippone et al., 1981; Lee, 2006) in a 2-D MOC calculation, and the polar angle set is chosen according to the TY quadrature (Yamamoto et al., 2007), which provides an accurate 2-D MOC calculation.

2.2. 2-D transport equation: method of characteristics (MOC)

Eq. (8) is integrated over the axial direction for computational plane k to obtain a 2-D transport equation, resulting in the following characteristic form of the transport equation,

$$\sin\theta_j \frac{\partial \psi_{g,j,k}(p)}{\partial p} + \sigma_{t,g}\psi_{g,j,k}(p) = q_{g,k}(p) - \xi_j \times \frac{\psi_{g,j,k+1/2}(p) - \psi_{g,j,k-1/2}(p)}{\Delta_k}, \tag{9}$$

where

$$\psi_{g,j,k}(p) = \frac{1}{\Delta_k}\int_{z_{k-1/2}}^{z_{k+1/2}} \psi_{g,j}(p,z)dz, \tag{9a}$$

$$\Delta_k = z_{k+1/2} - z_{k-1/2}, \tag{9b}$$

$$\psi_{g,j,k\pm1/2}(p) = \psi_{g,j}(p, z_{k\pm1/2}), \tag{9c}$$

$$q_{g,k}(p) = \frac{1}{\Delta_k}\int_{z_{k-1/2}}^{z_{k+1/2}} q_g(p,z)dz. \tag{9d}$$

The right-hand side of Eq. (9), which consists of the source term and the axial leakage term, is approximated as flat in a computational fine-mesh region. The computational mesh system consists of flat source regions (FSRs) in the radial direction, denoted by index m; therefore, the final 2-D transport equation in FSR m is written as follows:

$$\sin\theta_j \frac{\partial \psi_{g,j,k,m}(p)}{\partial p} + \sigma_{t,g,k,m}\psi_{g,j,k,m}(p) = q_{g,k,m} - L^z_{g,j,k,m}, \tag{10}$$

where

$$\sigma_{t,g,k,m} = \frac{1}{\Delta_k}\int_{z_{k-1/2}}^{z_{k+1/2}} \sigma_{t,g,m}(z)dz, \tag{10a}$$

$$L^z_{g,j,k,m} = \xi_j \frac{\psi_{g,j,k+1/2,m} - \psi_{g,j,k-1/2,m}}{\Delta_k}. \tag{10b}$$

The MOC planes are chosen to have homogeneous $\sigma_{t,g,k,m}$ in the k-th plane except for rodded meshes, and then Eq. (10) is solved by a conventional 2-D MOC solver described in the literature (Lee et al., 2000) for the given axial leakage obtained by a 1-D transport equation. The 1-D transport equation is derived in Section 2.3. A study of efficient methods by which to solve Eq. (10) (Roy, 1999; Lee et al., 2000; Yamamoto et al., 2004; Boyd et al., 2013, 2014; Kochunas, 2013) is not the scope of this paper.

2.3. 1-D transport equation: S_N

Eq. (8) is integrated over the radial direction for FSR m to obtain a 1-D transport equation, leading to the following 1-D transport equation,

$$\xi_j \frac{\partial \psi_{g,j,m}(z)}{\partial z} + \sigma_{t,g,k,m}\psi_{g,j,m}(z) = q_{g,m}(z) - \frac{1}{A_m}\int_{A_m} \sin\theta_j \frac{\partial \psi_{g,j}(p,z)}{\partial p}dA, \tag{11}$$

where

$$A_m = \text{mesh area for FSR } m, \tag{11a}$$

$$\psi_{g,j,m}(z) = \frac{1}{A_m}\int_{A_m} \psi_{g,j}(p,z)dA, \tag{11b}$$

$$q_{g,m}(z) = \frac{1}{A_m}\int_{A_m} q_g(p,z)dA. \tag{11c}$$

The radial leakage term in Eq. (11) is approximated by the axially averaged value obtained from the 2-D calculation. Thus, the final 1-D transport equation is obtained as follows:

$$\xi_j \frac{\partial \psi_{g,j,m}(z)}{\partial z} + \sigma_{t,g,k,m}\psi_{g,j,m}(z) = q_{g,m}(z) - L^r_{g,j,k,m}, \tag{12}$$

where

$$L^r_{g,j,k,m} = \frac{1}{A_m}\int_{A_m} \sin\theta_j \frac{\partial \psi_{g,j,k}(p)}{\partial p}dA = q_{g,k,m} - \xi_j \frac{\psi_{g,j,k+1/2,m} - \psi_{g,j,k-1/2,m}}{\Delta_k} - \sigma_{t,g,m}\psi_{g,j,k,m}, \tag{12a}$$

$$\psi_{g,j,k,m} = \frac{1}{A_m}\int_{A_m} \frac{\partial \psi_{g,j,k}(p)}{\partial p}dA. \tag{12b}$$

The radial leakage term, $L^r_{g,j,k,m}$, is obtained during the 2-D MOC calculation. To reduce the number of computational planes, Eq. (12) is solved by the linear characteristics (LC) scheme, which gives accurate results for the slab geometry (Alcouffe et al., 1979). During the 1-D calculation, the axial mesh, Δ_k, is divided into finer axial meshes called "sub-axial mesh" for the given source term to avoid a negative flux and increase the computational accuracy when the axial mesh size is rather large (e.g., larger than 10 cm).

Eqs. (10) and (12) are coupled by the radial and axial leakage terms; as a result, these equations are solved by an iterative approach.

2.4. Rod cusping correction: neighboring spectral index (NSI) weighting method

3-D transient problems usually involve control rods movement. When rods are partially inserted in a computational node, a proper cross-section homogenization technique for a partially rodded node (PRN) is needed. If a poor homogenization technique is used, the control rod worth would be very different from the reference value. For example, if a simple volume weight homogenization technique is used, the rod worth will differ greatly from the reference value, leading to significant computational error in the form of what is termed the rod cusping phenomenon (Joo, 1984). Homogenization techniques for conventional nodal methods, such as the approximate flux weighting method (Gehin, 1992), the bilinear weighting method (Kim and Cho, 1990), and the equivalent-node method (Dall'Osso, 2002) are not appropriate for 3-D heterogeneous problems, as techniques intended for

conventional nodal methods do not properly incorporate radial leakage effects.

However, 3-D heterogeneous transport problems should consider the radial leakage effects given that the usual mesh size in the radial direction is less than 1 cm, whereas the usual axial mesh size is larger than 5 cm. If the mesh sizes are compared to those used in conventional nodal methods, the radial mesh size is much smaller, as shown in Fig. 3. Therefore, the radial leakage effects would become relatively large in 3-D heterogeneous transport calculations. A simple and effective homogenization technique for a PRN for 3-D heterogeneous transport calculations, known as the inverse of spectral index (ISI) weighting method, was developed (Yamamoto, 2004) to reflect the radial leakage effects properly.

In the ISI weighting method, the scalar fluxes for the first groups (or the fast fluxes) in a PRN on the k-plane are estimated by the approximate flux weighting method, as follows:

$$\phi_{1,k,m}^{rod\text{-}in} = \frac{\Delta_{k+1}\phi_{1,k+1,m} + f_{in}\Delta_k\phi_{1,k,m}}{\Delta_{k+1} + f_{in}\Delta_k}, \tag{13}$$

and

$$\phi_{1,k,m}^{rod\text{-}out} = \frac{\Delta_{k-1}\phi_{1,k-1,m} + (1-f_{in})\Delta_k\phi_{1,k,m}}{\Delta_{k-1} + (1-f_{in})\Delta_k}, \tag{14}$$

where

$\phi_{1,k,m}^{rod\text{-}in}$ = estimated first group flux of the rodded region in the PRN (k-plane), (14a)

$\phi_{1,k,m}^{rod\text{-}out}$ = estimated first group flux of the unrodded region in the PRN (k-plane), (14b)

f_{in} = fraction of the rodded region in the PRN. (14c)

Then, the other group fluxes for the rodded and the unrodded regions in the PRN are estimated using the flux spectrum from a single-assembly calculation, as follows:

$$\phi_{g,k,m}^{rod\text{-}in} = \left(\phi_g^{rod\text{-}in,assembly}/\phi_1^{rod\text{-}in,assembly}\right)\cdot\phi_{1,k,m}^{rod\text{-}in}, \tag{15}$$

and

$$\phi_{g,k,m}^{rod\text{-}out} = \left(\phi_g^{rod\text{-}out,assembly}/\phi_1^{rod\text{-}out,assembly}\right)\cdot\phi_{1,k,m}^{rod\text{-}out}, \tag{16}$$

where

$\phi_g^{rod\text{-}in,assembly}$ = scalar flux in the rod cell obtained by the single-assembly calculation, (16a)

$\phi_g^{rod\text{-}out,assembly}$ = scalar flux in the unrodded cell obtained by the single-assembly calculation. (16b)

In the ISI weighting method, the ISI weighting factors for the rodded and the unrodded regions are calculated by a 2-D single-assembly calculation under all-reflective boundary conditions. Therefore, the ISI weighting method cannot reflect the spectrum interaction effect between adjacent fuel assemblies for the outer part of the fuel assembly (Yamamoto, 2004). In this study, the ISI weighting method is modified to take advantage of the 2-D/1-D fusion method. Different from the ISI weighting method, the flux spectrum in the PRN is estimated by the flux spectrum of neighboring meshes of the PRN during the 2-D/1-D calculations. Eqs. (17) and (18) below represent the modified fluxes for the rodded and the unrodded regions, respectively, in the PRN:

$$\phi_{g,k,m}^{rod\text{-}in} = (\phi_{g,k+1,m}/\phi_{1,k+1,m})\cdot\phi_{1,k,m}^{rod\text{-}in}, \tag{17}$$

and

$$\phi_{g,k,m}^{rod\text{-}out} = (\phi_{g,k-1,m}/\phi_{1,k-1,m})\cdot\phi_{1,k,m}^{rod\text{-}out}. \tag{18}$$

As shown in Eqs. (17) and (18), the flux spectrum for the rodded region is estimated by the flux spectrum of the nearest rodded mesh of the PRN, and the flux spectrum for the unrodded region is estimated by the flux spectrum of the nearest unrodded mesh of the PRN, as illustrated in Fig. 4. Since this method uses the neighboring spectrum indices, the method is named a neighboring spectral index (NSI) weighting method. In contrast to the original ISI method, the NSI weighing method does not require single-assembly calculations, as the 2-D/1-D fusion method

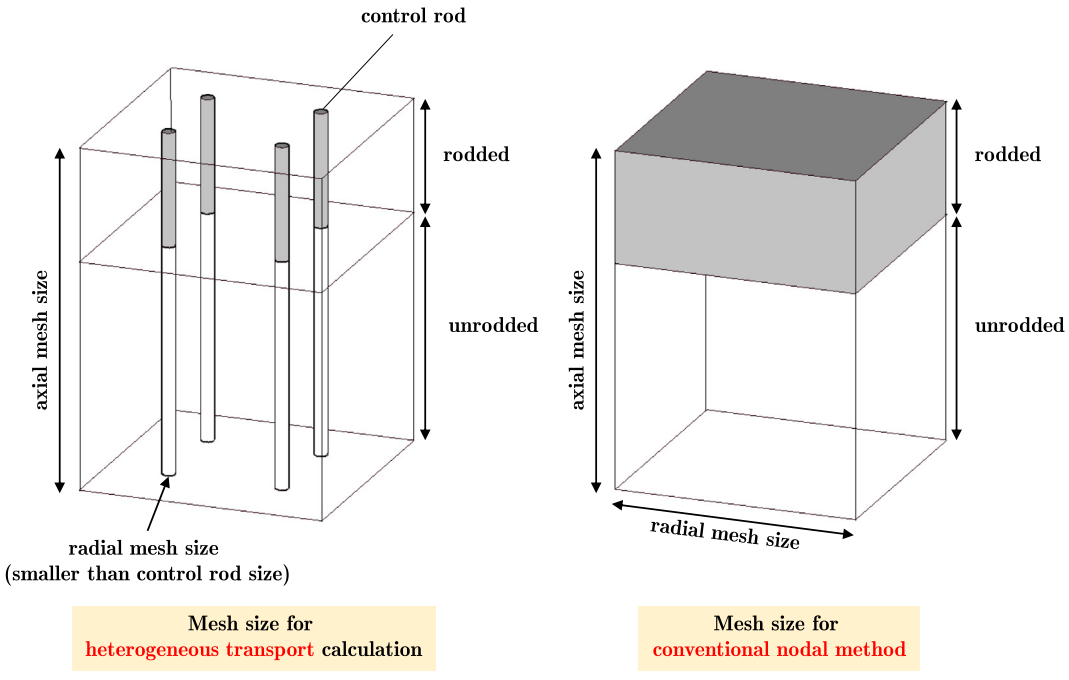

Fig. 3. Mesh size for heterogeneous transport calculation and conventional nodal method (not to scale).

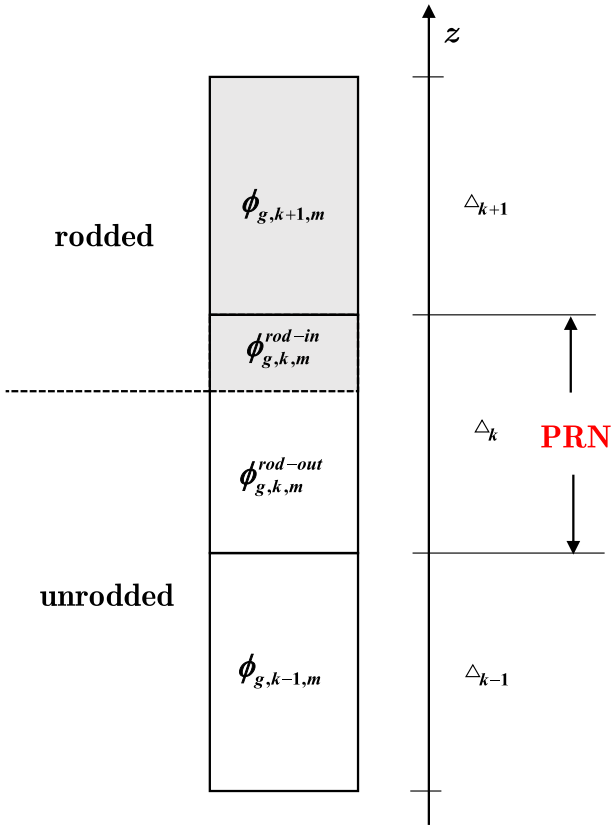

Fig. 4. Notations for neighboring spectral index (NSI) weighting method.

directly solves heterogeneous problems without a homogenization procedure. Additional computational burden is negligible, since the flux spectrums are saved during the 2-D/1-D calculations.

Using Eqs. (17) and (18), the homogenized cross sections of the PRN are obtained as follows:

$$\sigma_{x,g,k,m}=\frac{\sigma_{x,g,rod\text{-}in}f_{in}\phi^{rod\text{-}in}_{g,k,m}+\sigma_{x,g,rod\text{-}out}(1-f_{in})\phi^{rod\text{-}out}_{g,k,m}}{f_{in}\phi^{rod\text{-}in}_{g,k,m}+(1-f_{in})\phi^{rod\text{-}out}_{g,k,m}}, \tag{19}$$

where

$\sigma_{x,g,k,m}$ = homogenized cross-section of type x of the PRN, (19a)

$\sigma_{x,g,rod\text{-}in}$ = cross-section of type x for a rodded part, (19b)

$\sigma_{x,g,rod\text{-}out}$ = cross-section of type x for an unrodded part. (19c)

3. Transient p-CMFD methodology

To have the low-order form of the transport equation in a coarse mesh, Eq. (7) is homogenized, condensed, and integrated in coarse mesh I, resulting in the following form:

$$\sum_{u=x,y,z}\sum_{s=0,1}\frac{J^{+,I}_{G,u,s}(t_{n+1})-J^{-,I}_{G,u,s}(t_{n+1})}{H^I_u}+\sigma^I_{r,G}\phi^I_G(t_{n+1})=Q^I_G+\sum_{G'\neq G}\sigma^I_{s0,G'\to G}\phi^I_{G'}(t_{n+1}), \tag{20}$$

where

G = condensed group index, (20a)

H^I_u = coarse mesh size in direction u, (20b)

$$\phi^I_G=\frac{\sum_{k,m\in I}\sum_{g\in G}\phi_{g,k,m}A_mh_k}{\sum_{k,m\in I}A_mh_k}, \tag{20c}$$

h_k = mesh height in the k-plane, (20d)

$$\sigma^I_{x,G}=\frac{\sum_{k,m\in I}\sum_{g\in G}\phi_{g,k,m}\sigma_{x,g,k,m}A_mh_k}{\phi^I_G},\quad x=\text{reaction type}, \tag{20e}$$

$$Q^I_G=\left[(1-\beta^I)\chi^I_GF^I(t_{n+1})+\alpha^I_GF^I(t_{n+1})+S^I_{d,G}(t_n)\right]-\frac{1}{v^I_G}\times\frac{\phi^I_G(t_{n+1})-\phi^I_G(t_n)}{\Delta t_{n+1}}, \tag{20f}$$

$$\frac{1}{v^I_G}=\frac{\sum_{k,m\in I}\sum_{g\in G}\frac{\phi_{g,k,m}}{v_{g,k,m}}A_mh_k}{\phi^I_G}, \tag{20g}$$

$$F^I=\frac{1}{k_{eff}}\frac{\sum_{k,m\in I}A_mh_k\sum_{g'}\nu\Sigma_{f,g',k,m}\phi_{g',k,m}}{\sum_{k,m\in I}A_mh_k}, \tag{20h}$$

$$\chi^I_G=\frac{\sum_{k,m\in I}\sum_{g\in G}\chi_{g,k,m}A_mh_k\sum_{g'}\nu\Sigma_{f,g',k,m}\phi_{g',k,m}}{\sum_{k,m\in I}A_mh_k\sum_{g'}\nu\Sigma_{f,g',k,m}\phi_{g',k,m}}, \tag{20i}$$

$$\alpha^I_G=\frac{\sum_{k,m\in I}\sum_{g\in G}\alpha_{g,k,m}A_mh_k\sum_{g'}\nu\Sigma_{f,g',k,m}\phi_{g',k,m}}{\sum_{k,m\in I}A_mh_k\sum_{g'}\nu\Sigma_{f,g',k,m}\phi_{g',k,m}}, \tag{20j}$$

$$S^I_{d,G}=\frac{\sum_{k,m\in I}\sum_{g\in G}A_mh_kS_{d,g,k,m}}{\sum_{k,m\in I}A_mh_k}. \tag{20k}$$

The partial currents in Eq. (20) must preserve the net currents of the transport equation to have a consistent low-order equation. In this study, the partial currents are given by the p-CMFD formulation, as follows:

$$J^{+,I}_{G,u,s}=\frac{-\tilde{D}_{G,u,s}\left(\phi^{I^{s^*}}_G-\phi^I_G\right)+2\hat{D}^+_{G,u,s}\phi^I_G}{2}, \tag{21}$$

and

$$J^{-,I}_{G,u,s}=\frac{\tilde{D}_{G,u,s}\left(\phi^{I^{s^*}}_G-\phi^I_G\right)+2\hat{D}^-_{G,u,s}\phi^{I^{s^*}}_G}{2}, \tag{22}$$

where

I^{s^*} = coarse mesh index closest to the coarse mesh I at the surface s, (22a)

$\tilde{D}_{G,u,s}$ = arbitrary constant (usually chosen as the diffusion coupling coefficient), (22b)

and $\hat{D}^{\pm}_{G,u,s}$ are obtained from a "closure relation" in Eqs. (21) and (22) using the results from the high-order transport equation, the 2-D/1-D fusion kernel. The coarse mesh system in the radial direction is briefly illustrated in Fig. 5.

Substituting Eqs. (21) and (22) into Eq. (20), the following finite difference method (FDM) form of the p-CMFD equation is obtained:

$$-\sum_{u=x,y,z}\sum_{s=0,1}\left[\frac{(\tilde{D}_{G,u,s}+\hat{D}^-_{G,u,s})}{H^I_u}\phi^{I^{s^*}}_G(t_{n+1})\right]+\left[\sigma^I_{r,G}+\sum_{u=x,y,z}\sum_{s=0,1}\frac{(\tilde{D}_{G,u,s}+\hat{D}^+_{G,u,s})}{H^I_u}\right]\phi^I_G(t_{n+1})=Q^I_G+\sum_{G\neq G}\sigma^I_{s0,G'\to G}\phi^I_{G'}(t_{n+1}). \tag{23}$$

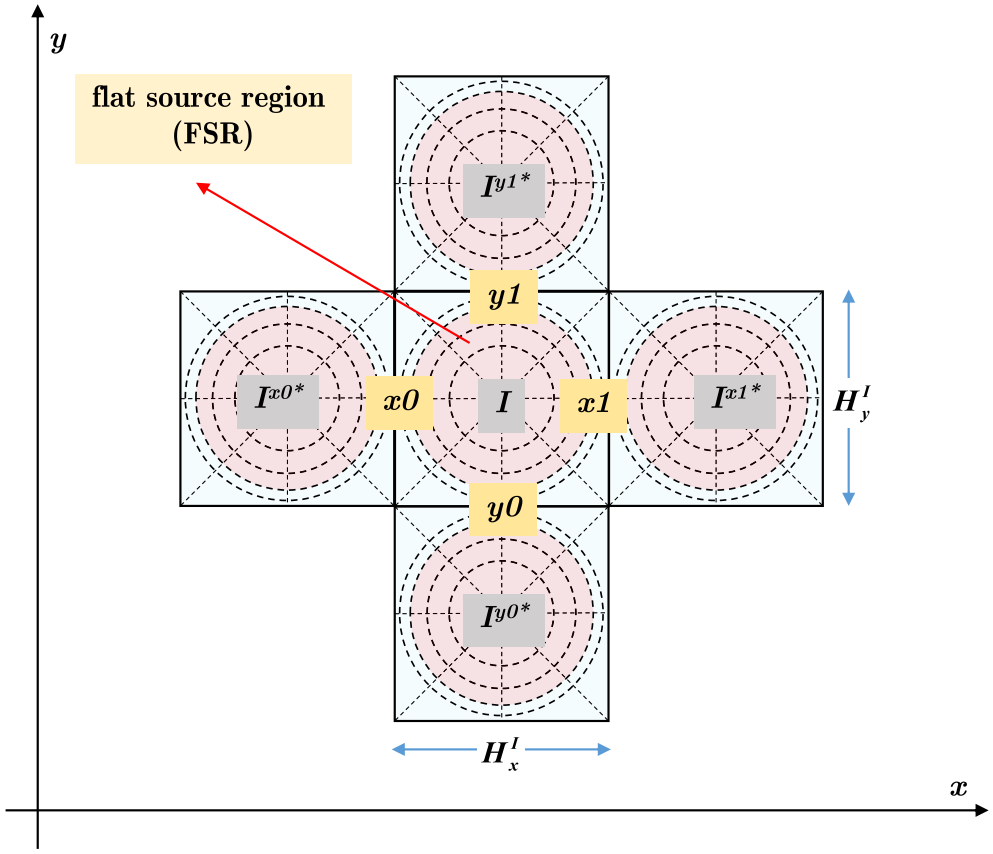

Fig. 5. Illustration of coarse and fine mesh systems in radial direction.

Eq. (23) can be solved by a conventional FDM solver. In this study, Gauss–Seidel method is used as the solver. The p-CMFD equation is typically used to accelerate the whole-core transport calculation; therefore, the resulting flux from the low-order equation is used to modulate the fission source term and other source terms. However, the p-CMFD equation can be used not only during the whole-core transport calculation as the accelerator, but also in the global/local iteration framework as the global wrapper or embedder of local problems. The role of the p-CMFD equation in the global/local iteration framework is discussed in Section 4.

4. Transient nonoverlapping local/global iterative method

In the local/global iteration framework, local transport problems and the global solver are "coupled" via local interface boundary conditions. The domain size of a local problem varies according to different local/global iteration frameworks. For example, the local domain of OLG iteration overlaps with the other domains, while NLG iteration has completely independent local domains. Both methods use the p-CMFD equation as the global wrapper (or embedder) of local problems, and NLG iteration has better computing performance during deterministic calculations than OLG iteration (Yuk et al., 2013). In this study, NLG iteration is chosen for the transient local/global iteration framework. Fig. 6 shows a schematic illustration of the NLG iteration process.

The main difference between "NLG iteration" and "whole-core p-CMFD acceleration" is whether the whole domain (whole-core) is decomposed into local domains or not. Their solvers are basically same; the 2-D/1-D fusion kernel is the local solver in NLG iteration, while it is the solver for the whole domain in whole-core p-CMFD acceleration. The p-CMFD equation is used as the global wrapper (or embedder) and the accelerator in NLG iteration, while it is used as the accelerator in whole-core p-CMFD acceleration.

4.1. Local transport calculation

The domain size of each local problem is a nonoverlapping region, and its size is usually the size of an assembly. Each local problem is solved by the 2-D/1-D fusion method (i.e., Eqs. (10) and (12)) with incoming angular fluxes as the boundary conditions. The boundary conditions of each local problem are updated by the previous global calculation. If the problem is in steady state, the multiplication factor k_{eff} is given from the previous global calculation.

Most of the computing time is consumed in the local transport calculation during the NLG iteration process; therefore, it is not desirable for the local transport calculation to fully converge at each local/global iteration step. To alleviate this computing time issue, the local transport calculations are solved with a fixed number of source iterations (only a few, around 1∼5); this is the conventional method used with whole-core transport acceleration by the p-CMFD equation or with other low-order equations. Therefore, the fission source and the other source terms are mainly updated by global calculations at the coarse-mesh level, whereas they are rarely updated by local transport calculations at the fine-mesh level.

4.2. Global calculation

A coarse mesh size can be chosen in an arbitrary way unless it introduces divergence, and the size is usually from the pin-cell size to the assembly size. If the coarse mesh size is small, it generally leads to smaller spectral radius than in the case of larger coarse

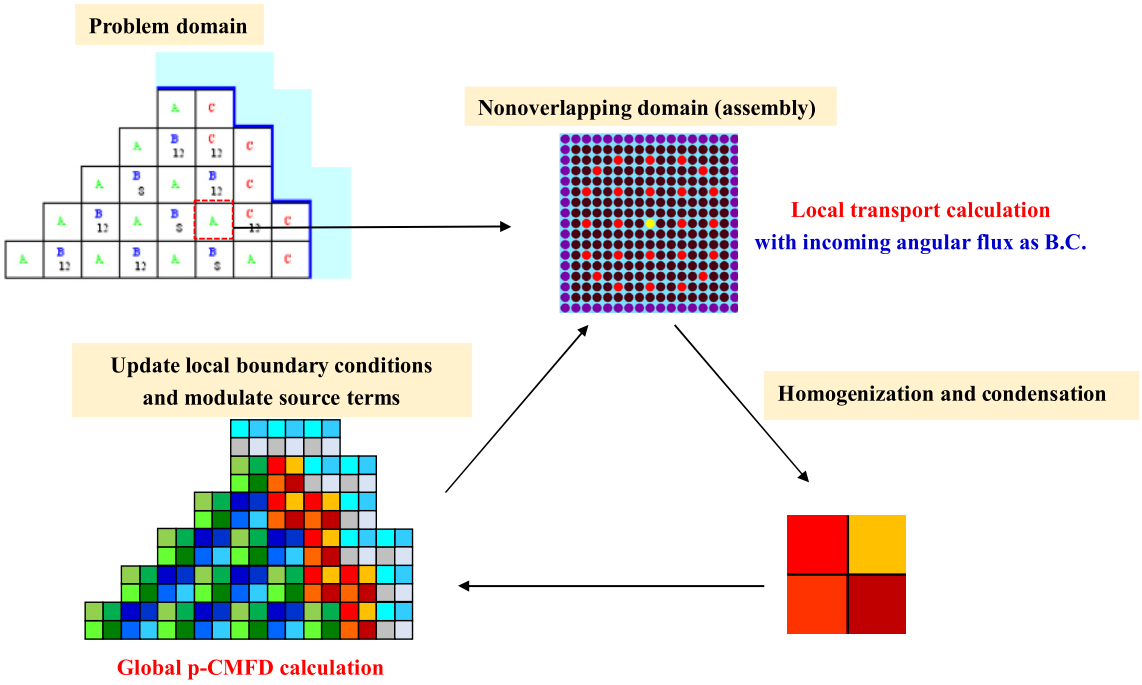

Fig. 6. Schematic illustration of nonoverlapping local/global (NLG) iteration.

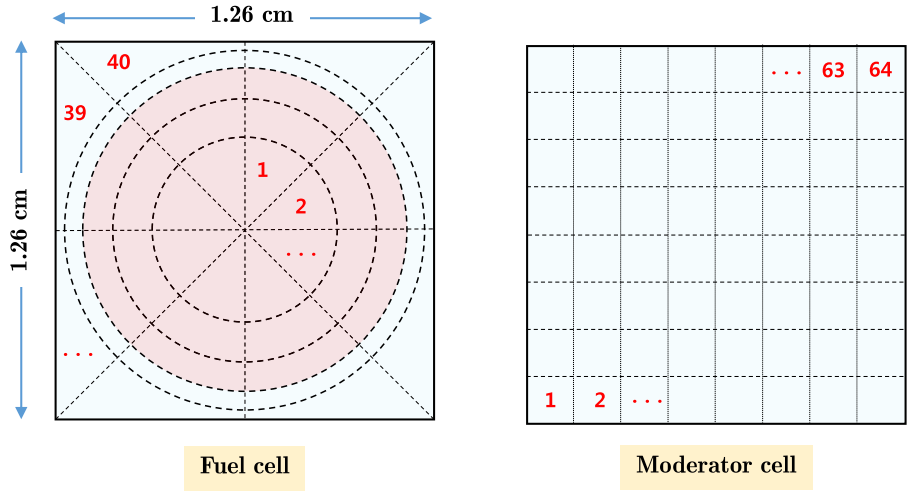

Fig. 7. Example of fine mesh system in fuel cell and moderator cell.

mesh size. However, a computing time consumed in solving the p-CMFD equation takes more as the coarse mesh size becomes smaller. In this study, we have chosen the coarse mesh size equal to the cell size based on the fact that the computing time consumed in solving the p-CMFD equation is quite smaller than that consumed in solving the local transport kernel. The impact of coarse mesh size on computing time is not the scope of this study. In the case of pin-cell size coarse mesh (PWR case: 1.26 cm by 1.26 cm), it usually contains dozens of fine mesh cells, as illustrated in Fig. 7.

The global wrapper (or embedder) in this study is the p-CMFD equation (i.e., Eq. (23)). The p-CMFD equation has several advantages as a global wrapper: 1) it provides the incoming transport partial currents at the local domain boundaries as solution results, and 2) it shows stable convergence in optically thick regions (Cho, 2012).

The p-CMFD equation solves the entire problem domain such that the solution reflects the inter-assembly transport effect. In other words, the correction factors, $\hat{D}^{\pm}$, in the p-CMFD equation preserve the incoming and outgoing transport partial currents at the interface of each local problem, and the global solution converges to the coarse-mesh-averaged transport solution.

4.3. Update of the local information

The global calculation solution is used to update the following local problem information: 1) the local boundary conditions, and 2) the fission source and transient source term.

The partial currents from the global calculation are used to update the incoming angular fluxes at each local problem boundary. Eq. (24) below represents the angular flux update at the local boundary:

$$\psi^{new}_{g,j,\partial D} = \frac{J^{-,I}_{G,s}}{J^{-,I,local}_{G,s}} \psi^{old}_{g,j,\partial D}, \tag{24}$$

where $g \in G$, ∂D lies on surface s, and the average incoming partial current of the local domain, $J^{-,I,local}_{G,s}$, is calculated from the outgoing partial current of the nearest neighbor node (i.e., $J^{-,I,local}_{G,s} = J^{+,I^{s^*},local}_{G,s}$). Note that the partial currents are the results of the p-CMFD equation. Hence, the p-CMFD equation is naturally appropriate when used to update the angular fluxes at the local boundaries.

The fission source term and transient source term are updated by modulated fluxes. The local fluxes are modulated as follows:

$$\phi^{new}_{g,k,m} = \frac{\phi^{I}_{G}}{\bar{\phi}^{I,local}_{G}} \phi^{old}_{g,k,m}, \tag{25}$$

where ϕ^{I}_{G} is the resulting flux from the p-CMFD equation, and $\bar{\phi}^{I,local}_{G}$ is the local coarse-mesh-averaged flux from the previous local transport calculation.

An overall flow diagram of the transient NLG iteration is illustrated in Fig. 8.

4.4. Pros and cons of NLG iteration

In the NLG iteration, all outgoing angular fluxes at the local boundaries must be stored as shown in Eq. (24). Therefore, the total memory requirement would be much larger if there were many local problems. However, NLG iteration is naturally suited for parallel computing, as all local problems are independent of each other and are "communicated" only via the global wrapper (the p-CMFD equation), for which the memory requirement is

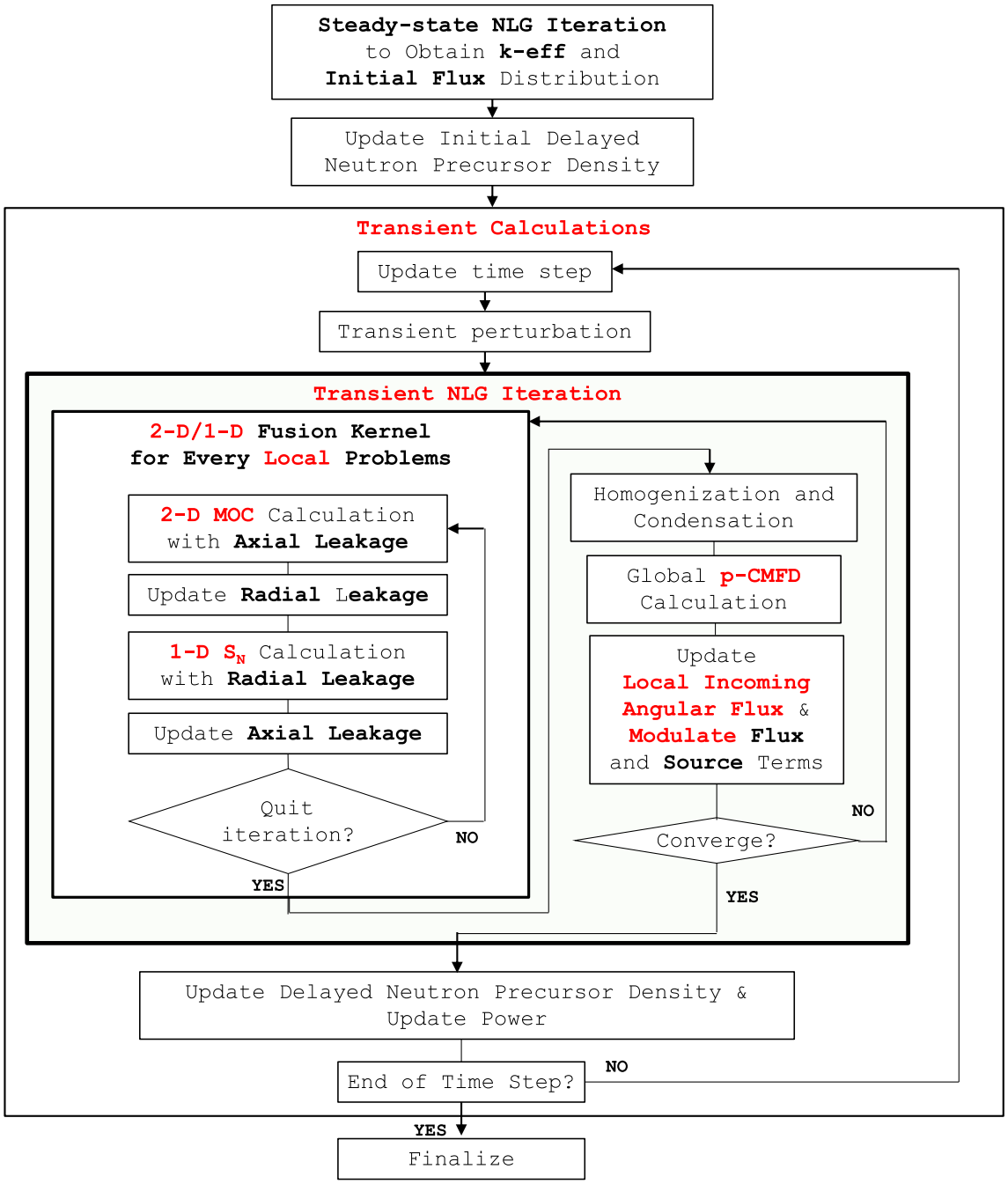

Fig. 8. Flow diagram of NLG iteration for transient calculation.

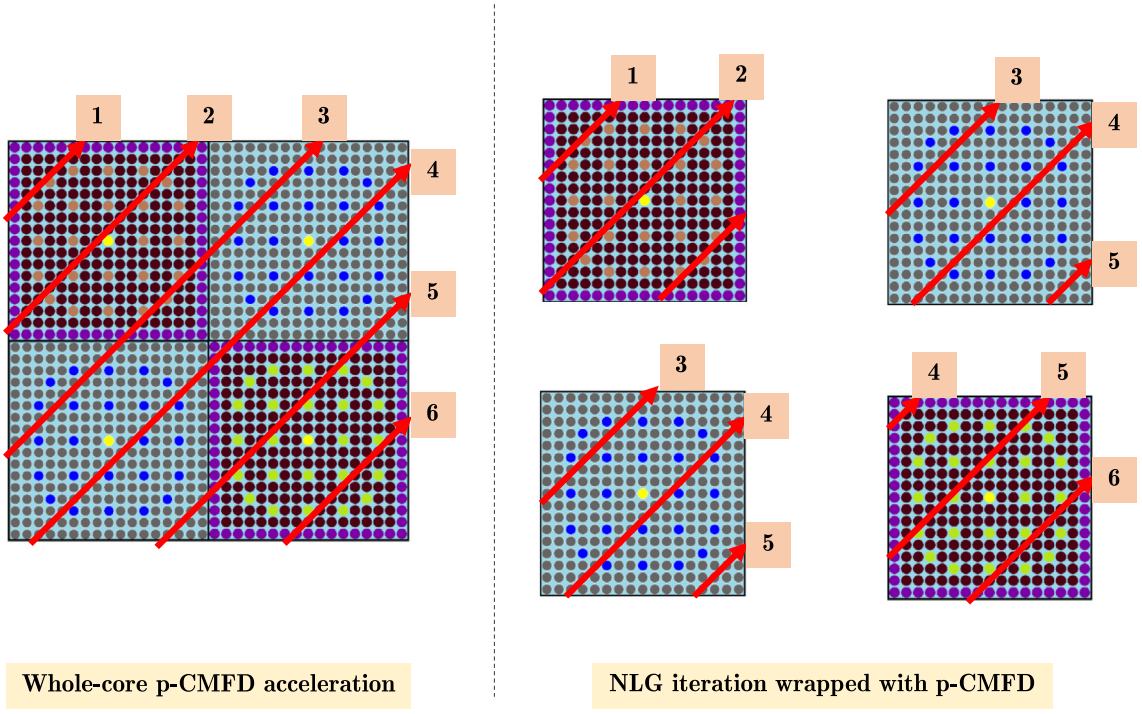

Fig. 9. Total track length comparison between the whole-core p-CMFD acceleration and the NLG iteration wrapped with p-CMFD.

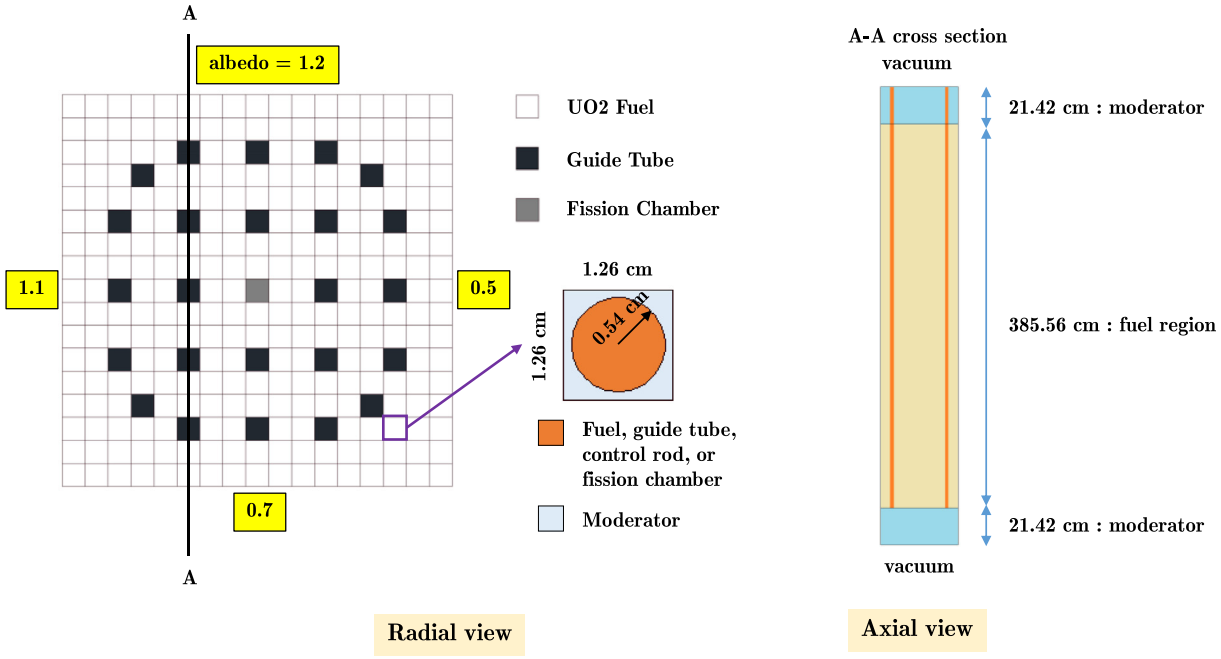

Fig. 10. Geometry of test problem 1.

relatively negligible compared to that for the local calculations. Therefore, the memory requirement issue for a large problem such as a whole-core PWR problem will not be serious if parallel computing nodes are used under a proper parallel protocol such as a message passing interface (MPI). In addition, the computing time will be shorter.

The computing time for the local calculations in the NLG iteration and that for the transport calculation in the whole-core p-CMFD acceleration "per iteration" are similar because the total domain size is identical in both cases, indicating that the total ray tracking lengths are the same, as illustrated in Fig. 9. However, the total number of iterations required to converge during the NLG iteration process would be greater than that for the whole-core p-CMFD acceleration, as the local problems are weakly coupled in the early stages of local/global iterations compared to whole-core p-CMFD acceleration. In addition, the local boundary incoming angular fluxes are modulated during NLG iteration; therefore, extra computing time is needed. As a result, the total

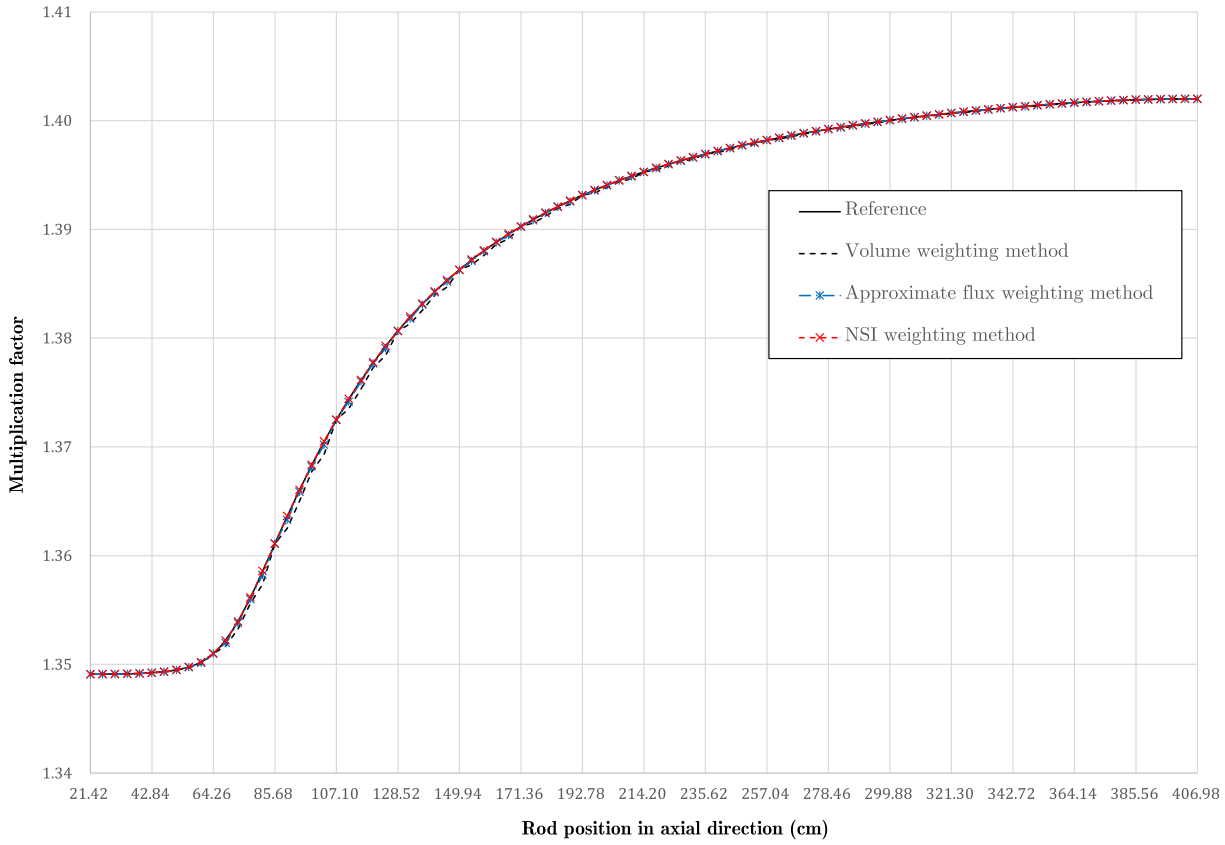

Fig. 11. Integral reactivity comparison.

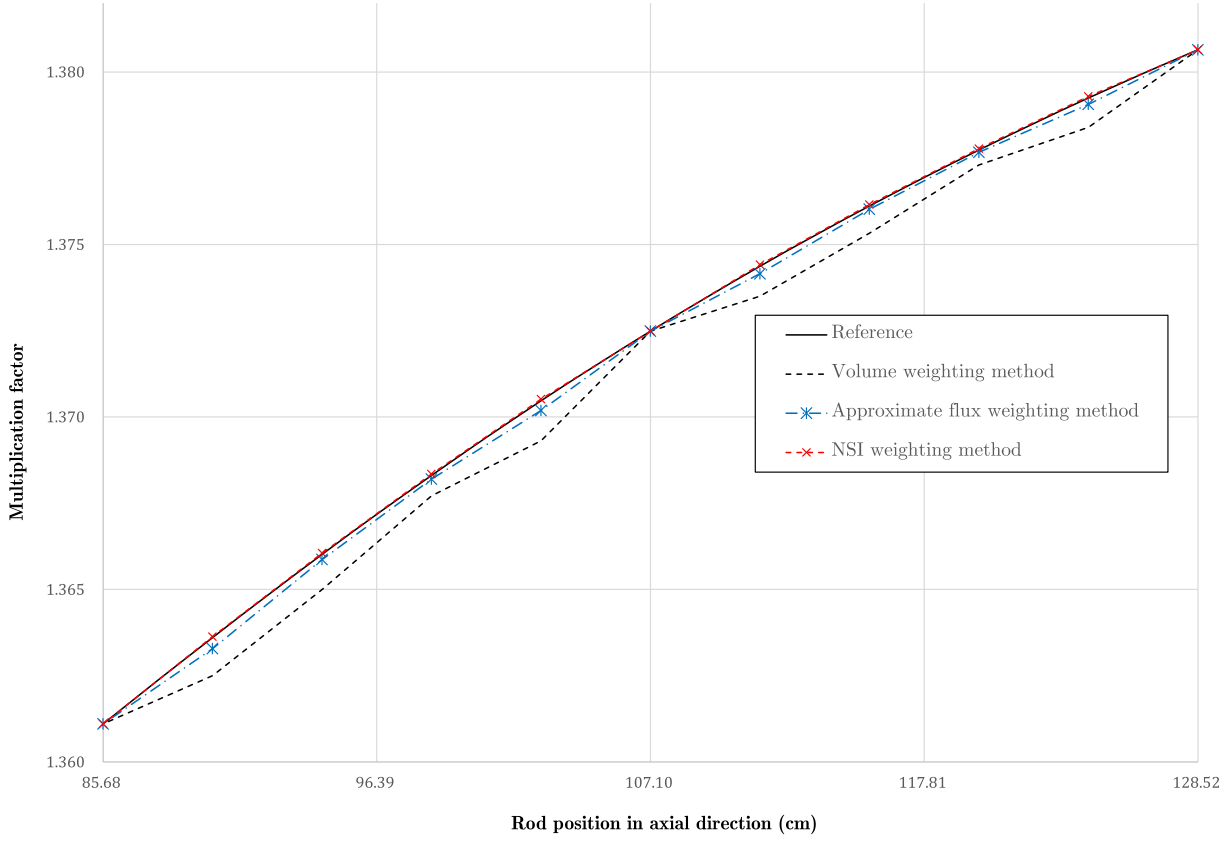

Fig. 12. Integral reactivity comparison from 85.68 to 128.52 cm.

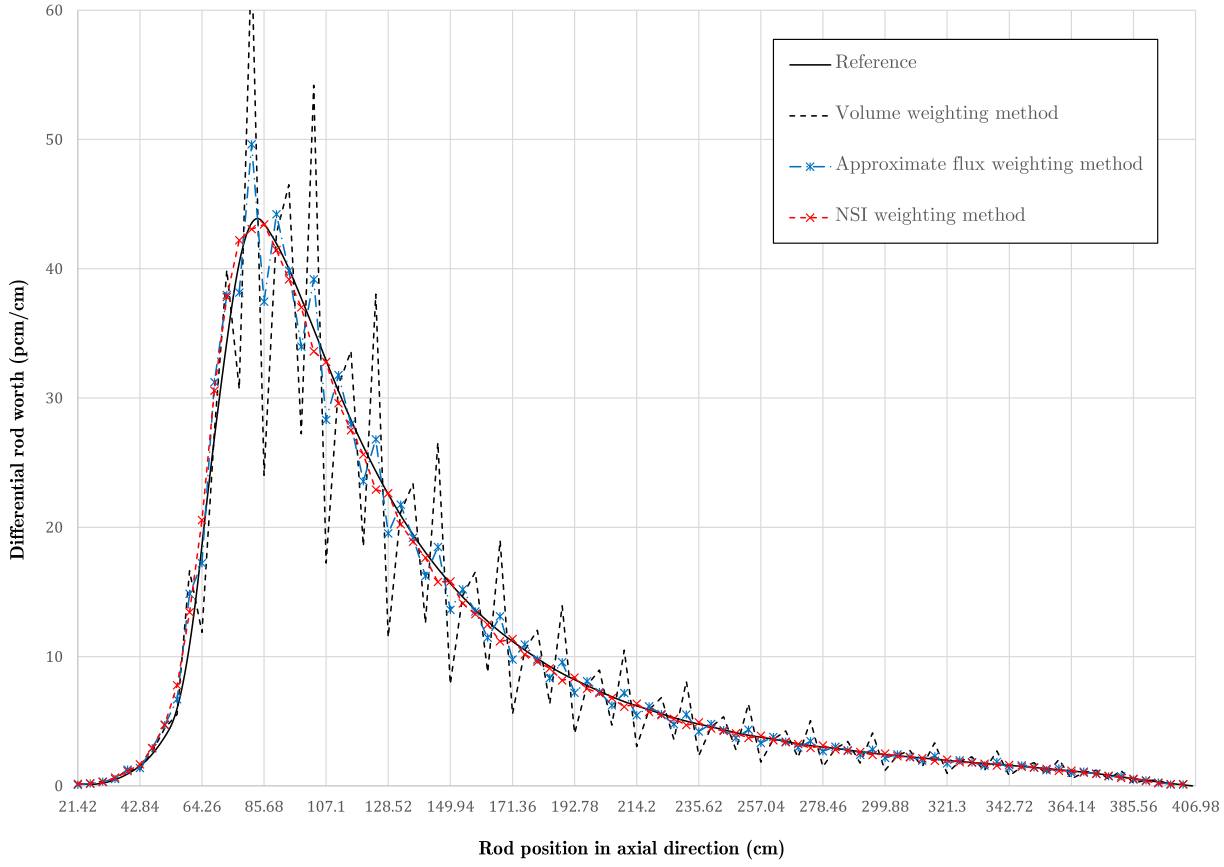

Fig. 13. Differential reactivity comparison.

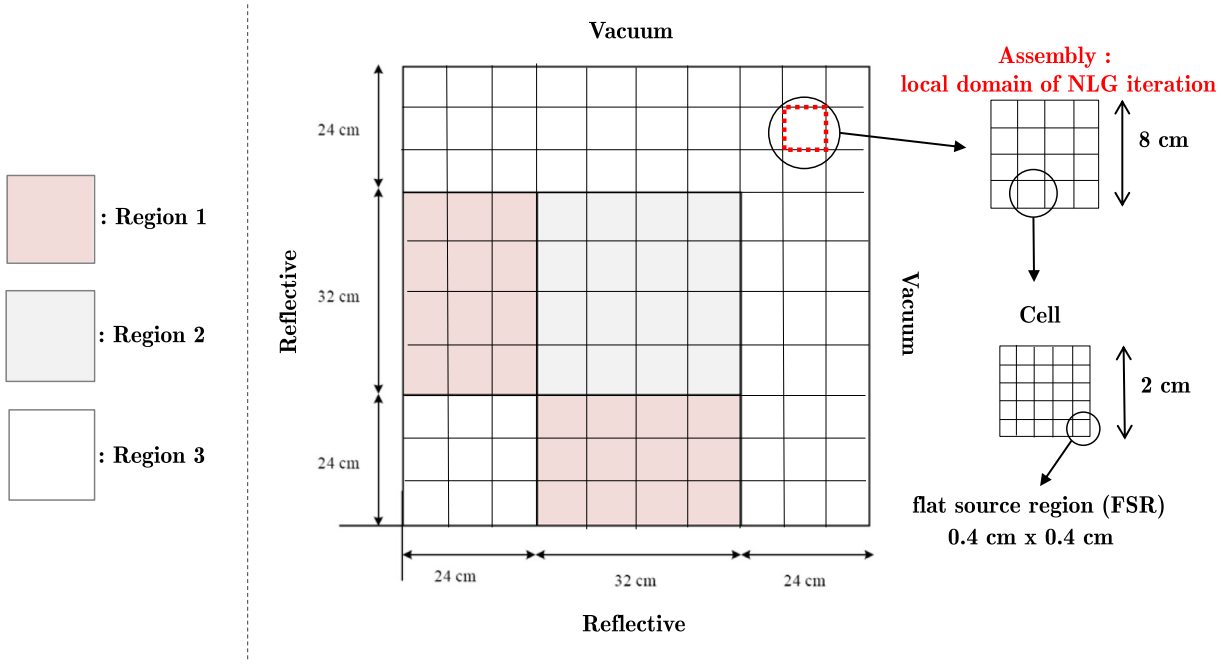

Fig. 14. Geometry and computational mesh system of test problem 2 (TWIGL).

computing time for NLG iteration would be longer than that for whole-core p-CMFD acceleration when a steady-state calculation is used. However, the gap is not overly large, and this process is still competitive with regard to whole-core p-CMFD acceleration (Yuk and Cho, 2014). Moreover, this issue would not be a significant problem with transient calculations given that the initial

Table 1
Transient perturbation of test problem 2 (TWIGL).

Initial		Final		Description
Time (s)	Composition	Time (s)	Composition	
0.0	1	0.2	4	Linear change
0.2	4	0.2	5	Step change
0.2	5	0.4	6	Linear change
0.4	6	0.4	1	Step change

Table 2
Cross sections of test problem 2 (TWIGL).

Composition	g	$\sigma_{t,g}$ [cm^{-1}]	$\nu\sigma_{f,g}$ [cm^{-1}]	χ_g	$\sigma_{s,g\to g'}$ [cm^{-1}]	
					$g'=1$	$g'=2$
1	1	0.23810	0.00700	1.00000	0.21810	0.01000
	2	0.83333	0.20000	0.00000	0.00000	0.68333
2	1	0.23810	0.00700	1.00000	0.21810	0.01000
	2	0.83333	0.20000	0.00000	0.00000	0.68333
3	1	0.25641	0.00300	1.00000	0.23841	0.01000
	2	0.66667	0.06000	0.00000	0.00000	0.61667
4	1	0.23810	0.00700	1.00000	0.21810	0.01000
	2	0.82983	0.20000	0.00000	0.00000	0.68333
5	1	0.23810	0.00700	1.00000	0.21810	0.01000
	2	0.83508	0.20000	0.00000	0.00000	0.68333
6	1	0.23810	0.00700	1.00000	0.21810	0.01000
	2	0.83683	0.20000	0.00000	0.00000	0.68333

Table 3
Delayed neutron precursors of test problem 2 (TWIGL).

Parameters	Values
Number of delayed neutron precursors	1
Decay constant (λ), s^{-1}	0.08
Delayed neutron fraction (β)	0.0064
Neutron velocity, cm/s	1.0E7, 1.0E5
Delayed neutron spectrum	1.0, 0.0

guess for NLG iteration at every computational time step comes from the results of the previous time step, which would be quite a good initial guess unless the reactivity change is rapid.

5. Numerical results with discussion

NLG iteration has been implemented in an in-house code, CRX-2K which has a transient calculation module, extending the static version CRX-2 (Yuk and Cho, 2015). In addition, whole-core p-CMFD acceleration has been implemented in the CRX-2K code to provide a reference solution such that NLG iteration can be compared to the reference calculation.

This section consists of four test problems; 1) a test problem to investigate the accuracy of the NSI weighing method, 2) a two-dimensional TWIGL type problem, 3) a three-dimensional homogeneous rodded-assembly ejection problem, and 4) a three-dimensional heterogeneous rod ejection problem. All problems except for the first problem involve transient perturbations. The capability of NLG iteration for the steady-state calculation was reported in an earlier study (Yuk and Cho, 2014).

5.1. Test problem 1: accuracy test for the NSI weighting method

Test problem 1 consists of a single UO_2 assembly, and the 7 group cross sections are sourced from the C5G7 benchmark problem (Smith et al., 2003). The geometry of this problem is described in Fig. 10, and there are four control rods in the problem. The axial mesh size is set to be 10.71 cm, and the arbitrary albedo boundary conditions are applied on each boundary side to have different flux spectrums in each rod. Note that rod worth difference between a fully-inserted case (21.42 cm) and a fully-out case (409.98 cm) is around 5000 pcm which is a little exaggerated, and this exaggeration is intended to see the capability of the neighboring spectral index (NSI) weighing method.

All rods are fully inserted (21.42 cm) in fuel regions initially. Four different calculations were carried out to investigate the accuracy of the NSI weighting method. The first one is reference, and all

Table 4
Calculation conditions of test problem 2 (TWIGL).

	Variant-K	DeCART	CRX-2K	
			Whole-core p-CMFD acceleration	NLG iteration
Transport solver	Variational nodal method	MOC	MOC	MOC
Accelerator or global wrapper	N/A[a]	CMFD	p-CMFD	p-CMFD
Time discretization	Fully implicit 0.01/0.002	Adaptive theta 0.01/0.005	Fully implicit 0.01	Fully implicit 0.01
Polar angle set	N/A	N/A	TY quadrature	TY quadrature
Number of polar angles per octant	N/A	4	3	3
Average ray width (cm)	N/A	0.02	~0.02	~0.02
Fission source error criteria	N/A	N/A	10^{-5}	10^{-5}

[a] Detailed input description is not available, or it is not needed.

Table 5
Result summary of test problem 2 (TWIGL).

	Variant-K[a]	DeCART	CRX-2K	
			Whole-core p-CMFD acceleration	NLG iteration
Multiplication factor (k_{eff})	0.91605	0.91609	0.91612	0.91612
Δk_{eff} [b]	Reference	−4 pcm	−7 pcm	−7 pcm
Calculation time (s)[c] in steady-state calculation	N/A[d]	N/A	933	1002
Number of local/global iterations	N/A	N/A	18	18
Memory requirement (MB)	N/A	N/A	169	797
Calculation time (s) in transient calculations	N/A	N/A	13217	14022

[a] Reference.
[b] Reference − result.
[c] Intel Xeon X5670 @ 2.93 GHz is used.
[d] Information is not available.

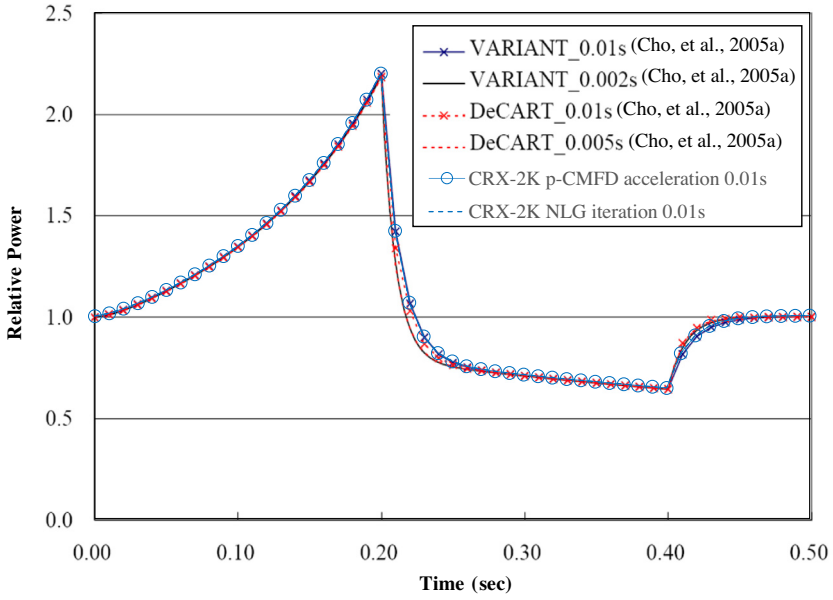

Fig. 15. Power vs time: test problem 2 (TWIGL).

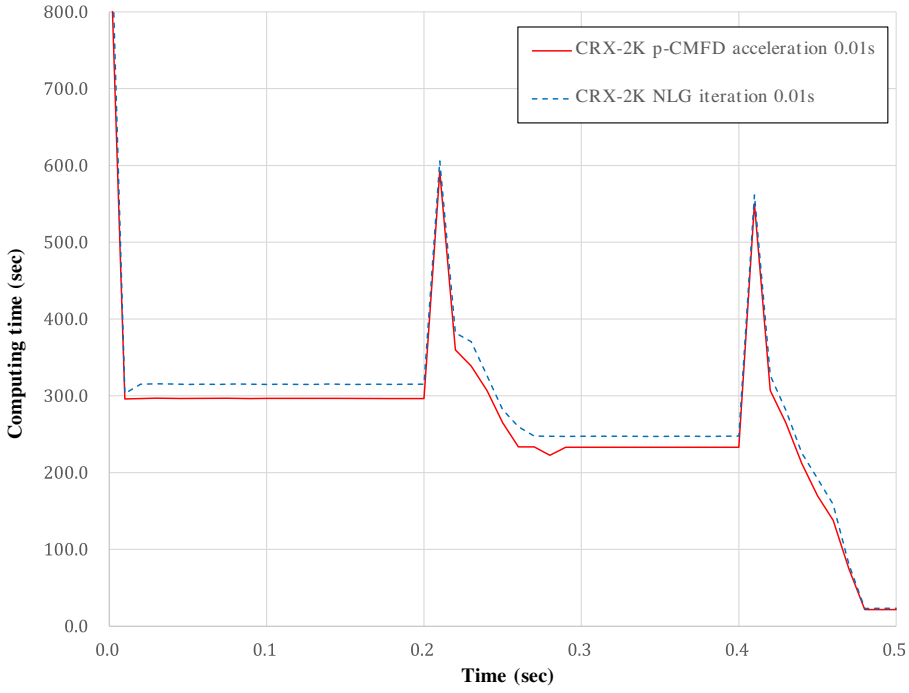

Fig. 16. Computing time vs time: test problem 2 (TWIGL).

rods are inserted in every 10.71 cm (i.e., 21.42, 32.13, 42.84,..., 406.98 cm). Therefore, the control rod tips are consistent with the axial mesh boundary, so no rod cusping phenomenon occurs. k_{eff} from the reference is interpolated by cubic spline. The second one is the volume weighting method, the third one is the approximate flux weighing method (Gehin, 1992), and the fourth one is the NSI weighing method. For the second one to the fourth one, the rods are inserted in every 4.28 cm.

Fig. 11 shows the integral reactivity effects of the control rods, and Fig. 12 shows the enlargement of integral reactivity effect between 85.68 and 128.52 cm. Fig. 13 shows the differential reactivity effects of the control rods. As shown in the results, the volume weighting method causes the largest rod cusping phenomenon among the results. The approximate flux weighing method reduces the rod cusping phenomenon a lot compared to the volume weighting method, but a large oscillation in the differential reactivity still remains. In contrast to these methods, the newly proposed NSI method shows accurate k_{eff} and a smooth differential reactivity trend.

5.2. Test problem 2: TWIGL problem

Test problem 2 is a TWIGL problem (Hageman and Yasinsky, 1969). The purpose of test problem 2 is to check whether NLG

Table 6
Comparison of regional power densities of test problem 2 (TWIGL).

Time (s)	Region	Variant-K[a]	DeCART	Error (%)[b]	CRX-2K			
					Whole-core p-CMFD acceleration	Error (%)	NLG iteration	Error (%)
0	1	1.5699	1.5703	−0.03	1.5700	−0.01	1.5700	−0.01
	2	1.9935	1.9941	−0.03	1.9940	−0.03	1.9940	−0.03
	3	0.4506	0.4504	0.04	0.4504	0.04	0.4504	0.04
0.1	1	1.5937	1.5938	−0.01	1.5938	−0.01	1.5938	−0.01
	2	1.9815	1.9822	−0.04	1.9821	−0.03	1.9821	−0.03
	3	0.4491	0.4487	0.09	0.4488	0.07	0.4488	0.07
0.2	1	1.6183	1.6184	−0.01	1.6183	0.00	1.6183	0.00
	2	1.9690	1.9696	−0.03	1.9695	−0.03	1.9695	−0.03
	3	0.4475	0.4472	0.07	0.4473	0.04	0.4473	0.04
0.3	1	1.5363	1.5365	−0.01	1.5365	−0.01	1.5365	−0.01
	2	2.0109	2.0115	−0.03	2.0113	−0.02	2.0113	−0.02
	3	0.4526	0.4524	0.04	0.4524	0.04	0.4524	0.04
0.4	1	1.5255	1.5256	−0.01	1.5257	−0.01	1.5257	−0.01
	2	2.0165	2.0170	−0.02	2.0170	−0.02	2.0170	−0.02
	3	0.4533	0.4530	0.07	0.4530	0.07	0.4530	0.07
0.5	1	1.5699	1.5689	0.06	1.5700	−0.01	1.5700	−0.01
	2	1.9935	1.9947	−0.06	1.9940	−0.03	1.9940	−0.03
	3	0.4506	0.4504	0.04	0.4504	0.04	0.4504	0.04

[a] Reference.
[b] (Reference − result)/reference × 100.

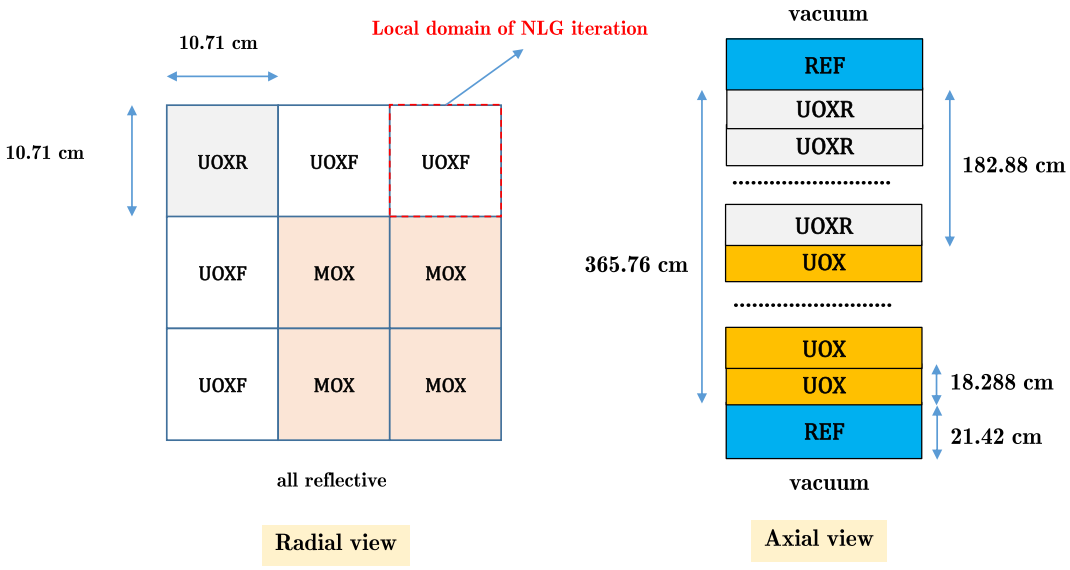

Fig. 17. Geometry of test problem 3 (Mini-Core 3D).

Table 7
Cross sections of test problem 3 (Mini-Core 3D).

Composition	g	$\sigma_{t,g}$ [cm^{-1}]	$\nu\sigma_{f,g}$ [cm^{-1}]	χ_g	$\sigma_{s,g\to g'}$ [cm^{-1}]	
					$g'=1$	$g'=2$
MOX	1	2.40844E−01	7.30698E−03	1.000000	2.13856E−01	1.48498E−02
	2	9.03803E−01	2.92500E−01	0.00000	0.00000E+00	6.98771E−01
UOXF	1	2.42628E−01	7.62590E−03	1.000000	2.15199E−01	1.74866E−02
	2	8.79010E−01	1.57892E−01	0.00000	0.00000E+00	7.60676E−01
UOX	1	2.39594E−01	6.08060E−03	1.000000	2.11972E−01	1.70480E−02
	2	9.07752E−01	1.56260E−01	0.00000	0.00000E+00	7.92581E−01
UOXR	1	2.30113E−01	5.91172E−03	1.000000	2.00510E−01	1.34085E−02
	2	8.88279E−01	1.64057E−01	0.00000	0.00000E+00	7.37376E−01
Reflector	1	3.01887E−01	0.00000E+00	1.000000	2.71935E−01	2.75262E−02
	2	1.22567E+00	0.00000E+00	0.00000	0.00000E+00	1.18843E+00

Table 8
Delayed neutron precursors of test problem 3 (Mini-Core 3D).

Parameters	Values	
Number of delayed neutron precursors	6	
Decay constant (λ), s^{-1}	Family index	Value
	1	0.01280
	2	0.03180
	3	0.11900
	4	0.31810
	5	1.40270
	6	3.92860
Delayed neutron fraction (β)	Family index	Value
	1	0.00026
	2	0.00152
	3	0.00139
	4	0.00307
	5	0.00110
	6	0.00026
Neutron velocity, cm/s	1.0E7, 1.0E5	
Delayed neutron spectrum	1.0, 0.0	

iteration with the 2-D MOC kernel works well in transient calculations. This problem consists of homogeneous assemblies, and the geometry and the computational mesh system are illustrated in Fig. 14. The local problem size is set to 8 cm by 8 cm for the NLG iteration process. The transient perturbation is determined by the linear change of the cross sections in region 1 in time, as given in Table 1, and the corresponding cross sections are given in Table 2. The information of the delayed neutron precursors is given in Table 3. The results by CRX-2K are compared to the results by other transport codes, Variant-K (Rineiski and Doriath, 1997) and DeCART (Joo et al., 2004), and the results by the other codes are available in the literature (Cho et al., 2005b). The conditions are set to give accurate results, and they are given in Table 4.

Table 5 shows the result summary. As shown in the results, the multiplication factors are identical for both NLG iteration and whole-core p-CMFD acceleration, and the differences from Variant-K and DeCART are small. The number of iterations required to converge for NLG iteration for the steady-state calculation is same with whole-core p-CMFD acceleration in this problem.

Figs. 15 and 16, and Table 6 show the transient results of test problem 2, with the results of CRX-2K overlaid on the results given in the report (Cho et al., 2005b). The results according to NLG iteration and whole-core p-CMFD acceleration are also identical within the numerical error criteria in the transient calculations. The computing time for NLG iteration takes longer than that for whole-core p-CMFD acceleration, but the computing time difference between them becomes smaller when the reactivity is not changed (between 0.4 and 0.5 s in this problem). Note that parallel computation has not been implemented. In addition, the results are similar to those by the other transport codes. From this problem, it can be said that the NLG iteration with the 2-D MOC kernel works properly.

5.3. Test problem 3: Mini-Core 3D problem

Test problem 3 is the Mini-Core 3D Problem (Lee et al., 2004). Test problem 3 is used to check whether NLG iteration with the 2-D/1-D fusion kernel works well with transient calculations. This problem also consists of homogeneous assemblies and is three-dimensional in space, as illustrated in Fig. 17. The local problem size is set to half of the assembly size (10.71 cm) for the NLG iteration process. The transient perturbation is determined by the

Table 9
Calculation conditions of test problem 3 (Mini-Core 3D).

	Variant-K	DeCART	CRX-2K	
			Whole-core p-CMFD acceleration	NLG iteration
Transport solver	Variational nodal method	2-D: MOC 1-D: Diffusion	2-D: MOC 1-D: S_N	2-D: MOC 1-D: S_N
Accelerator or global wrapper	N/A[a]	CMFD	p-CMFD	p-CMFD
Time discretization	Fully implicit 0.001	Fully implicit 0.002	Fully implicit 0.002	Fully implicit 0.002
Polar angle set	N/A	N/A	TY quadrature	TY quadrature
Number of polar angles per octant	N/A	4	3	3
Average ray width (cm)	N/A	0.02	~0.08	~0.08
Axial mesh size (cm) (reflector/fuel)	21.42/18.288	21.42/18.288	10.71/9.144	10.71/9.144
Rod cusping correction	Volume weighting method	Volume weighting method	NSI weighting method	NSI weighting method
Fission source error criteria	N/A	N/A	10^{-5}	10^{-5}

[a] Detailed input description is not available, or it is not needed.

Table 10
Result summary of test problem 3 (Mini-Core 3D).

	Variant-K[a]	DeCART	CRX-2K	
			Whole-core p-CMFD acceleration	NLG iteration
Multiplication factor (k_{eff})	1.08026	1.08019	1.08019	1.08019
Δk_{eff} [b]	Reference	−7 pcm	−7 pcm	−7 pcm
Calculation time (s)[c] in steady-state calculation	N/A[d]	N/A	3371	4367
Number of local/global iterations	N/A	N/A	36	43
Memory requirement (GB)	N/A	N/A	3.4	4.2
Calculation time (h) in transient calculations	N/A	N/A	46.0	55.6

[a] Reference.
[b] Reference − result.
[c] Intel Xeon X5670 @ 2.93 GHz is used.
[d] Information is not available.

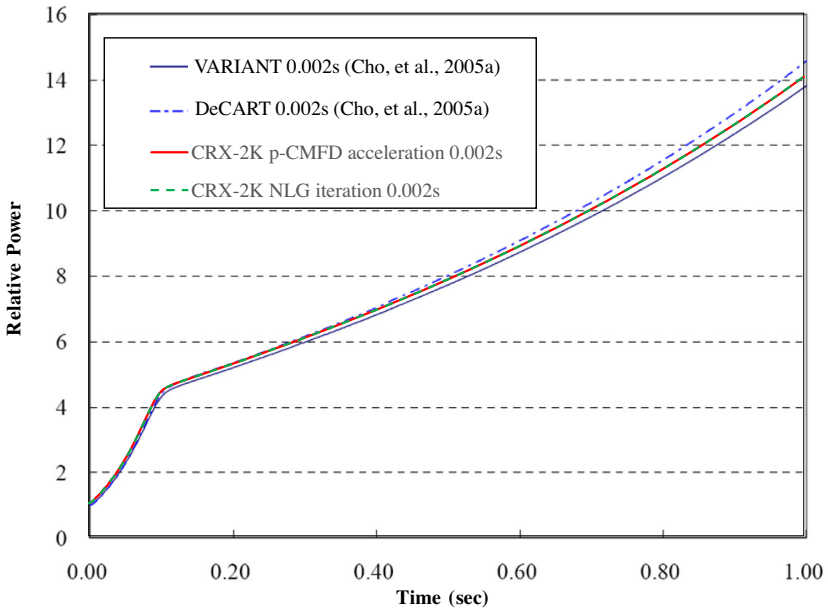

Fig. 18. Power vs time: test problem 3 (Mini-Core 3D).

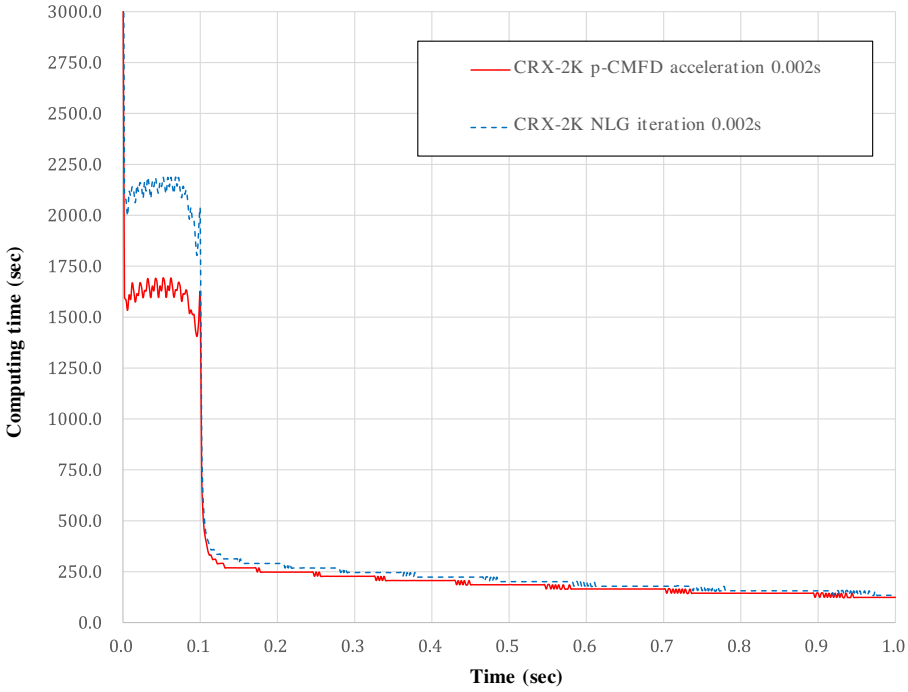

Fig. 19. Computing time vs time: test problem 3 (Mini-Core 3D).

ejection of the UOX assembly in 0.1 s. The cross sections and the information pertaining to the delayed neutron precursors are given in Tables 7 and 8, and the calculation conditions are given in Table 9. The rod cusping phenomenon would be negligible in this problem because the assemblies are already homogeneous. Note that both Variant-K and DeCART use the volume weighting method for the rod cusping correction.

The result summary is in Table 10. The multiplication factors are identical for both NLG iteration and whole-core p-CMFD acceleration, as expected, and they are in good agreement with the results by the other transport codes. In this problem, the computing time in the steady-state calculation for NLG iteration takes approximately 1.3 times more than that consumed in whole-core p-CMFD acceleration. This is due to the MOX fuels used, as MOX fuels lead to steep flux gradients at the fuel interfaces. These steep gradients are not well taken care of by NLG iteration in the early stages of the local/global iterations, because the local domains are relatively weakly coupled compared to those in whole-core p-CMFD acceleration. However, this difference would be lessened (or reversed) and NLG iteration is expected to be faster than whole-core p-CMFD acceleration if parallel computation is implemented in a future update of CRX-2K.

Table 11
Comparison of assembly power densities of test problem 3 (Mini-Core 3D).

Time (s)	Assembly	Variant-K[a]	DeCART	Error (%)[b]	CRX-2K			
					Whole-core p-CMFD acceleration	Error (%)	NLG iteration	Error (%)
0.0	UOXR	0.9125	0.9120	−0.06	0.9123	−0.02	0.9123	−0.02
	UOXF	1.0279	1.0280	0.01	1.0272	−0.06	1.0272	−0.06
	MOX	0.9939	0.9940	0.01	0.9947	0.08	0.9947	0.08
0.2	UOXR	0.9743	0.9750	0.07	0.9739	−0.04	0.9739	−0.04
	UOXF	1.0267	1.0270	0.03	1.0260	−0.07	1.0260	−0.07
	MOX	0.9797	0.9800	0.03	0.9805	0.08	0.9805	0.08
0.4	UOXR	0.9743	0.9750	0.07	0.9740	−0.03	0.9740	−0.03
	UOXF	1.0267	1.0270	0.02	1.0260	−0.07	1.0260	−0.07
	MOX	0.9797	0.9800	0.03	0.9805	0.08	0.9805	0.08
0.6	UOXR	0.9743	0.9750	0.07	0.9740	−0.03	0.9740	−0.03
	UOXF	1.0267	1.0270	0.02	1.0260	−0.07	1.0260	−0.07
	MOX	0.9797	0.9800	0.03	0.9805	0.08	0.9805	0.08
0.8	UOXR	0.9743	0.9750	0.07	0.9740	−0.03	0.9740	−0.03
	UOXF	1.0267	1.0270	0.02	1.0260	−0.07	1.0260	−0.07
	MOX	0.9797	0.9800	0.03	0.9805	0.08	0.9805	0.08
1.0	UOXR	0.9743	0.9750	0.07	0.9740	−0.03	0.9740	−0.03
	UOXF	1.0267	1.0270	0.02	1.0260	−0.07	1.0260	−0.07
	MOX	0.9797	0.9800	0.03	0.9805	0.08	0.9805	0.08

[a] Reference.
[b] (Reference − result)/reference × 100.

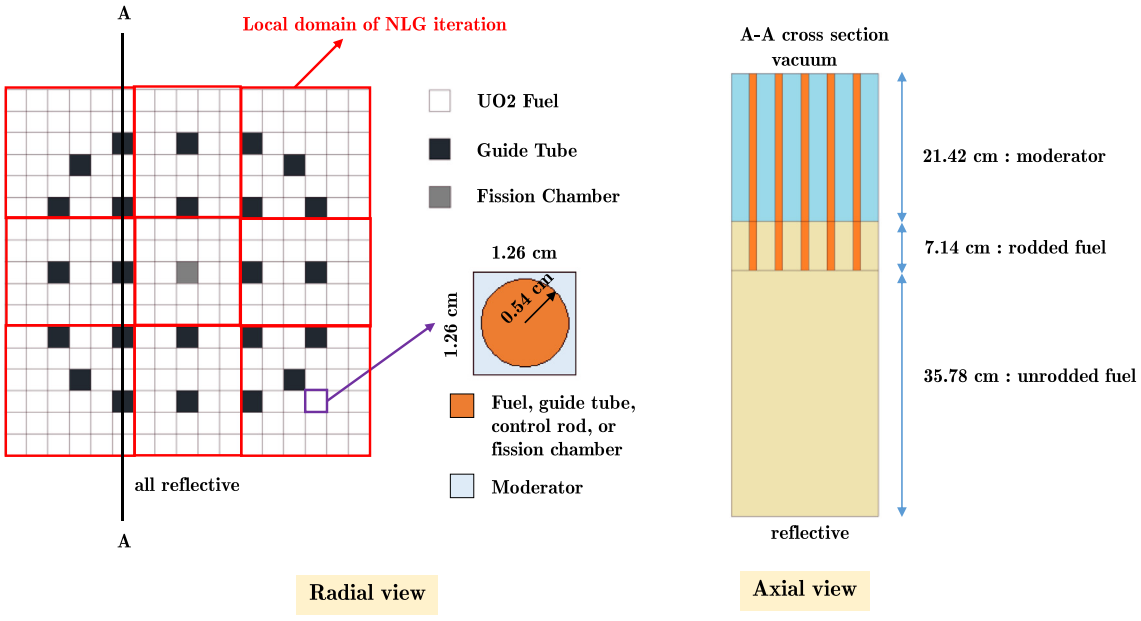

Fig. 20. Geometry of test problem 4 (heterogeneous UO_2 fuel assembly).

Table 12
Calculation conditions of test problem 4 (heterogeneous UO_2 fuel assembly).

	CRX-2K	
	Whole-core p-CMFD acceleration	NLG iteration
Transport solver	2-D: MOC, 1-D: S_N	
Accelerator or global wrapper	p-CMFD	
Time discretization	Fully implicit, 0.002	
Polar angle set	TY quadrature	
Number of polar angles per octant	3	
Average ray width (cm)	~0.08	
Axial mesh size (cm)	3.57	
Fission source error criteria	10^{-5}	

Figs. 18 and 19, and Table 11 show the transient results of test problem 3, with the results of CRX-2K overlaid on the results given in the report (Cho et al., 2005b). As expected, the results by NLG iteration and whole-core p-CMFD acceleration are identical, and they show trends similar to those of the other transport codes. The computing time for the transient calculations of NLG iteration becomes similar to that of whole-core p-CMFD acceleration as the transient calculations go on. Especially after 0.1 s, when the reactivity is not changed, the computing time is almost same in both cases, and this means that NLG iteration becomes quite comparable in terms of computing time if a good initial guess at a time step is given from a previous time step. The transient capability of the

Table 13
Steady-state results of test problem 4 (heterogeneous UO_2 fuel assembly).

	CRX-2K	
	Whole-core p-CMFD acceleration	NLG iteration
Multiplication factor (k_{eff})	1.27239	1.27239
Calculation time (s)[a] in steady-state calculation	1600	2010
Number of global iterations	35	39
Memory requirement (GB)	1.9	2.3
Calculation time (h) in transient calculations	10.8	13.4

[a] Intel Xeon X5670 @ 2.93 GHz is used.

NLG iteration of the CRX-2K code is verified through test problems 3 and 4.

5.4. Test problem 4: heterogeneous UO_2 fuel assembly problem

Test problem 4 is more challenging. This problem was devised to determine the transient capability of NLG iteration for a 3-D heterogeneous problem. This problem consists of a single UO_2 assembly, but the fuel rods are described with heterogeneity in their geometry, as illustrated in Fig. 20. This is a seven-group problem, and the cross sections in the C5G7 benchmark problem (Smith et al., 2003) are used. The information pertaining to delayed neutron precursors is sourced from an earlier study (Boyarinov et al.,

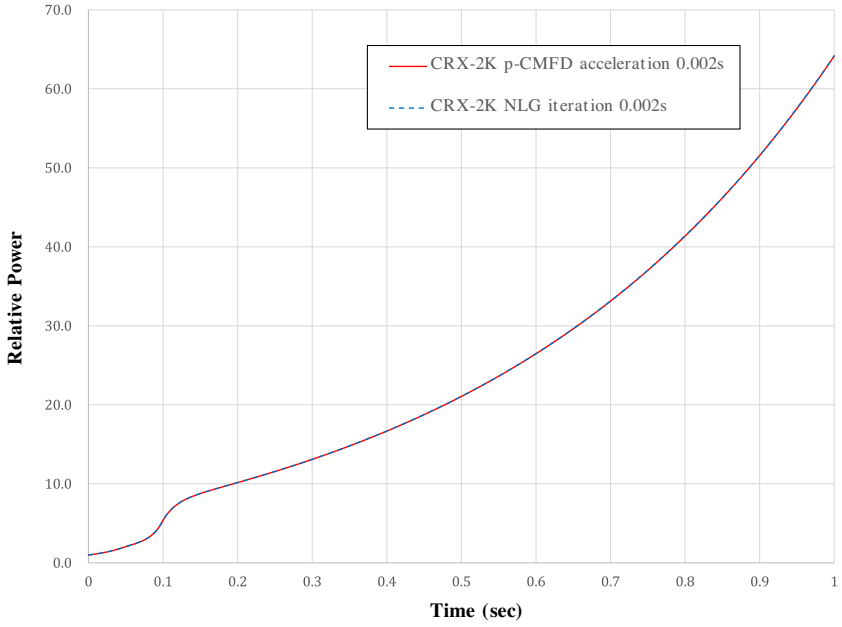

Fig. 21. Power vs time: test problem 4 (heterogeneous UO_2 fuel assembly).

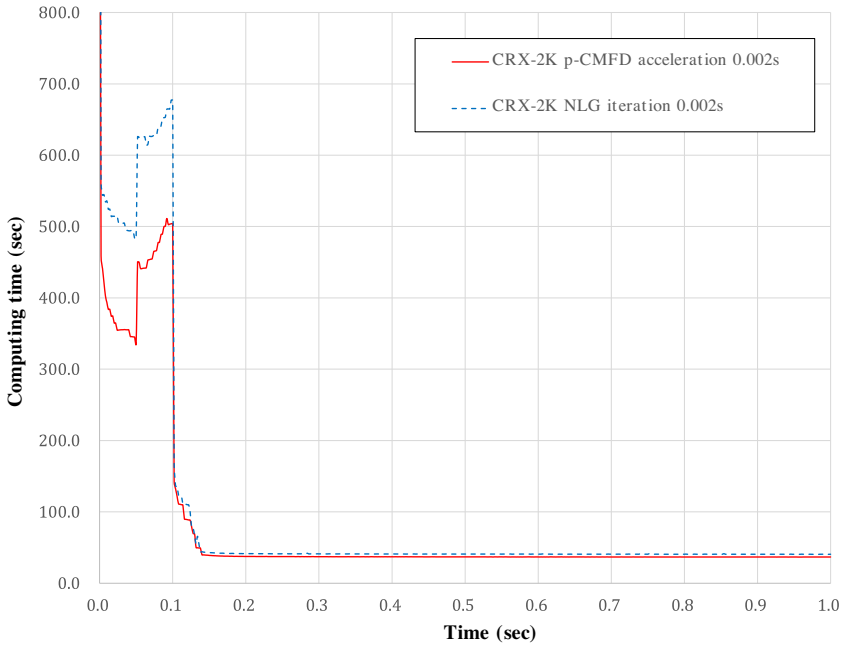

Fig. 22. Computing time vs time: test problem 4 (heterogeneous UO_2 fuel assembly).

2014). For NLG iteration, the single assembly is divided into nine local problems, and each local domain is enclosed by the red lines as shown in Fig. 20. The details of the cross sections and the delayed neutron precursors are omitted for the sake of brevity. The control rods are initially inserted into the active core to a distance of 7.14 cm, and the transient perturbation is established by control rod ejection in 0.1 s. The rod worth is enough (Δk_{eff} = 796 pcm) to result in a fast transient trend. The calculation conditions are given in Table 12.

The results are summarized in Table 13. NLG iteration for a heterogeneous problem takes 1.26 times more than whole-core p-CMFD acceleration in terms of the computing time. The multiplication factors are identical for both cases, as expected.

Figs. 21 and 22 show the transient results of test problem 4. As shown in Fig. 21, the results follow the trend of the rod ejection problem, as shown in test problem 3, and both NLG iteration and whole-core p-CMFD acceleration give identical results. As in test problem 3, the computing time of NLG iteration becomes more competitive with whole-core p-CMFD acceleration as the reactivity has no changes as shown in Fig. 22.

From test problem 4, the transient calculation capability of NLG iteration for a heterogeneous problem is shown. However, the results are not compared to the results by other transport codes, considering that this type of 3-D heterogeneous transient transport problem is not reported in the literature.

NLG iteration takes more computing time than whole-core p-CMFD acceleration in all test problems, still less than 2 times, while the computing time of NLG iteration becomes more competitive with whole-core p-CMFD acceleration in the interval of no or small reactivity changes. Moreover, if parallel computation is implemented in the local kernel, NLG iteration would become faster than whole-core p-CMFD acceleration.

With regard to memory requirements, all three problems show no significant differences for NLG iteration and whole-core p-CMFD acceleration, because they have relatively small domains compared to a realistic reactor core. It is expected that memory requirements will become a serious issue in practical applications. Thus, parallel computation will be an unavoidable choice, and NLG iteration will be quite advantageous.

6. Conclusions and future works

NLG iteration has been extended to deal with transient 3-D transport problems. The local problem is solved by the 2-D/1-D fusion transport method, and the local problems are coupled by the global wrapper of the p-CMFD equation. In addition, to lessen the rod cusping phenomenon for a problem involving a rod ejection scenario, the neighboring spectral index (NSI) weighting method is introduced to take the advantage of the benefits of the 2-D/1-D fusion method. The transient NLG method has been implemented in the in-house code, CRX-2K.

First test problem shows that the NSI weighting method is accurate and lessens the rod cusping phenomenon significantly compared to the volume weighting method and the approximate flux weighting method. In addition, the NSI method naturally reflects the spectrum interaction effect between adjacent assemblies, in contrast to the ISI method.

The other three transient problems, including a 3-D heterogeneous problem, are also computed. The results show that 1) the solution by NLG iteration is identical within the numerical error criteria to the solution by whole-core p-CMFD acceleration in both steady-state and transient cases, and 2) NLG iteration takes more computing times (still less than 2 times) than whole-core p-CMFD acceleration, because a parallel protocol has not been used yet to solve local problems. However, the computing time for NLG iteration becomes more competitive in transient calculations when there is no or small reactivity changes, as the good initial guess at a time step comes from the results of the previous time step.

The main disadvantages of NLG iteration would be 1) an additional memory requirement for the local boundary angular fluxes, and 2) a slower computing speed compared to that for whole-core p-CMFD acceleration. These disadvantages will disappear (or be reversed), however, if a proper parallel protocol such as MPI is used to solve each local problem in parallel computing nodes. Note that further parallelization of discretized angles can be achieved in a single computing node with several computing cores by a shared memory parallel architecture such as OpenMP. Therefore, NLG iteration can be parallelized both in space domain and in discretized angles.

As future works, the following areas are identified; 1) parallelization for transient NLG iteration implemented in CRX-2K and 2) test of CRX-2K on realistic and large power reactor core problems.

Acknowledgement

This work was supported in part by a National Research Foundation (NRF) of Korea grant funded by the Korean government (Ministry of Science, ICT and Future Planning) (No. 2015M2B2A9029928).

References

Alcouffe, R.E., Larsen, E.W., Miller Jr., W.F., Wienke, B.R., 1979. Computational efficiency of numerical methods for the multigroup, discrete-ordinates neutron transport equations: the slab geometry case. Nucl. Sci. Eng. 71, 111.

Boyarinov, V.F., Kondrushin, A.E., Fomichenko, P.A., 2014. Benchmark on deterministic time-dependent transport calculations without spatial homogenisation. In: PHYSOR 2014, Kyoto, Japan, September 28–October 3, 2014.

Boyd, W., Smith, K., Forget, B., 2013. A massively parallel method of characteristic neutral particle transport code for GPUs. In: Proc. Int. Conf. Mathematics and Computational Methods Applied to Nuclear Science and Engineering, Sun Valley, Idaho, USA, May 5–9, 2013.

Boyd, W., Shaner, S., Li, L., Forget, B., Smith, K., 2014. The OpenMOC method of characteristics neutral particle transport code. Ann. Nucl. Energy 68, 43.

Cho, N.Z., 2012. The partial current-based CMFD (p-CMFD) method revisited. Trans. Kor. Nucl. Soc., Gyeongju, Korea, October 25–26, 2012, <http://www.kns.org/kns_files/kns/file/229%C1%B6%B3%B2%C1%F8.pdf>.

Cho, N.Z., Lee, G.S., Park, C.J., 2002. Fusion of method of characteristics and nodal method for 3-D whole-core transport calculation. Trans. Am. Nucl. Soc. 86, 322.

Cho, N.Z., Lee, G.S., Park, C.J., 2003. Partial current-based CMFD acceleration of the 2D/1D fusion method for 3D whole-core transport calculations. Trans. Am. Nucl. Soc. 88, 594.

Cho, J.Y., Kim, K.S., Lee, C.C., Zee, S.Q., 2005a. Transient capability of the DeCART code. KAERI, KAERI/TR-2930, 2005a.

Cho, J.Y., Kim, K.S., Lee, C.C., Joo, H.G., Yang, W., Taiwo, T.A., Thomas, J., 2005b. Transient capability for a MOC-based whole core transport code DeCART. Trans. Am. Nucl. Soc. 92, 721.

Cho, N.Z., Yuk, S., Yoo, H.J., Yun, S., 2013. Overlapping local/global iteration framework for whole-core transport solution. Nucl. Sci. Eng. 175, 227.

Clarno, K.T., Adams, M.L., 2005. Capturing the effects of unlike neighbors in single-assembly calculations. Nucl. Sci. Eng. 149, 182.

Dall'Osso, A., 2002. Reducing rod cusping effect in nodal expansion method calculations. In: Proc. Int. Conf. New Frontiers of Nuclear Technology: Reactor Physics, Safety and High-Performance Computing, Seoul, Korea, October 7–10, 2002.

Filippone, W.L., Woolf, S., Lavigne, R.J., 1981. Particle transport calculations with the method of streaming rays. Nucl. Sci. Eng. 77, 119.

Gehin, J.C., 1992. A quasi static polynomial nodal method for nuclear reactor analysis (Ph.D. thesis). Massachusetts Institute of Technology.

Hageman, L.A., Yasinsky, J.B., 1969. Comparison of alternating-direction time-differencing methods with other implicit methods for the solutions of the neutron group-diffusion equations. Nucl. Sci. Eng. 38, 8.

Hoogenboom, J.E., Martin, W.R., Petrovic, B., 2010. Monte Carlo performance benchmark for detailed power density calculation in a full size reactor core. Benchmark specifications revision 1.1, June 2010, <http://www.nea.fr/dbprog/MonteCarloPerformanceBenchmark.htm>.

Joo, H.S., 1984. Resolution of the control rod cusping problem for nodal methods (Ph.D. thesis). Massachusetts Institute of Technology.

Joo, H.G., Barber, D.A., Jiang, G., Downar, T.J., 1998. PARCS: Purdue advanced reactor core simulator PU/NE-98-26. Purdue University.

Joo, H.G., Cho, J.Y., Kim, K.S., Lee, C.C., Zee, S.Q., 2004. Methods and performance of a three-dimensional whole-core transport code DeCART. In: PHYSOR 2004, Chicago, Illinois, USA, April 25–29, 2004.

Kelley, B.W., Larsen, E.W., 2012. CMFD acceleration of spatial domain-decomposed neutron transport problems. In: PHYSOR 2012, Knoxville, Tennessee, USA, April 15–20, 2012.

Kim, Y.H., Cho, N.Z., 1990. A bilinear weighting method for the control rod cusping problem in nodal methods. J. Korean Nucl. Soc. 22, 238.

Kim, H.R., Cho, N.Z., 1993. Global/local iterative methods for equivalent diffusion theory parameters in nodal calculations. Ann. Nucl. Energy 20, 767.

Kochunas, B.M., 2013. A hybrid parallel algorithm for the 3-D method of characteristics solution of the Boltzmann transport equation on high performance computer clusters (Ph.D. thesis). University of Michigan.

Lee, G.S., 2006. Development of 2-D/1-D fusion method for three-dimensional whole-core heterogeneous neutron transport calculations (Ph.D. thesis). Korea Advanced Institute of Science and Technology.

Lee, G.S., Cho, N.Z., 2006. 2D/1D fusion method solutions of the three-dimensional transport OECD benchmark problem C5G7 MOX. Prog. Nucl. Energy 48, 410.

Lee, G.S., Cho, N.Z., Hong, S.G., 2000. Acceleration and parallelization of the method of characteristics for lattice and whole-core heterogeneous calculations. In: PHYSOR 2000, Pittsburgh, USA, May 7–11, 2000.

Lee, D., Kozlowski, T., Downar, T., Lee, C., Lee, H.C., 2004. Application of SP_3 approximation to MOX transient analysis in PARCS. Trans. Am. Nucl. Soc. 91, 252.

Lewis, E.E., Miller Jr., W.F., 1984. Computational methods of neutron transport. John Wiley & Sons.

Rahnema, F., 1989. Boundary condition perturbation theory for use in spatial homogenization methods. Nucl. Sci. Eng. 102, 183, see also Corrigendum, *Nucl. Sci. Eng.* **104**, 89 (1990).

Rahnema, F., McKinley, M.S., 2002. High-order cross-section homogenization method. Ann. Nucl. Energy 29, 875.

Rineiski, A., Doriath, J.Y., 1997. Time-dependent neutron transport with variational nodal method. In: Proc. Joint Int. Conf. on Math. Methods and Supercomputing for Nuclear Application, Saratoga Springs, New York, USA, October, 1997, p. 1661.

Roy, R., 1999. The cyclic characteristics method with anisotropic scattering. In: Proc. Int. Conf. Mathematics and Computation, Reactor Physics and Environmental Analysis in Nuclear Applications, Madrid, Spain, September 27–30, 1999, p. 1224.

Seubert, A., Velkov, K., Langenbuch, S., 2008. The time-dependent 3-D discrete ordinates code TORT-TD with thermal-hydraulic feedback by ATHLET models. In: PHYSOR 2008, Interlaken, Switzerland, September 14–19, 2008.

Smith, K.S., Rhodes III, J.D., 2000. CASMO characteristics method for two-dimensional PWR and BWR core calculation. Trans. Am. Nucl. Soc. 88, 294.

Smith, M.A., Lewis, E.E., Na, B-C., 2003. Benchmark on deterministic transport calculations without spatial homogenization: A 2-D/3-D MOX fuel assembly 3-D benchmark, NEA/NSC/DOC(2003) 16. Organization for Economic Co-operation and Development, Nuclear Energy Agency.

Sutter, H., 2005. The free lunch is over: a fundamental turn toward concurrency in software. Dr. Dobb's J. 30, 3, <http://www.gotw.ca/publications/concurrency-ddj.htm>.

Talamo, A., 2013. Numerical solution of the time dependent neutron transport equation by the method of the characteristics. J. Comput. Phys. 240, 248.

Taylor, J.B., Baratta, A.J., 2009. A time-dependent method of characteristics for 3D nuclear reactor kinetics applications. In: Proc. Int. Conf. Mathematics Computation and Reactor Physics, Saratoga, USA, 2009.

Yamamoto, A., 2004. A simple and efficient control rod cusping model for three-dimensional pin-by-pin core calculations. Nucl. Technol. 145, 11.

Yamamoto, A., Kitamura, Y., Yamane, Y., 2004. Computational efficiencies of approximated exponential functions for transport calculations of the characteristics method. Ann. Nucl. Energy 31, 1027.

Yamamoto, A., Tabuchi, M., Sugimura, N., Ushio, T., Mori, M., 2007. Derivation of optimum polar angle quadrature set for the method of characteristics based on approximation error for the Bickley function. J. Nucl. Sci. Technol. 44, 129.

Yoo, H.J., Imron, M., Cho, N.Z., 2015. Whole-core transport solution via deterministic S_N transport/p-CMFD overlapping local/global calculation in hexagonal geometry problem. Ann. Nucl. Energy 75, 468.

Yuk, S., Cho, N.Z., 2014. p-CMFD acceleration and nonoverlapping local/global iterative transport methods with 2-D/1-D fusion kernel. In: PHYSOR 2014, Kyoto, Japan, September 28–October 3, 2014.

Yuk, S., Cho, N.Z., 2015. Whole-core transport solutions with 2-D/1-D fusion kernel via p-CMFD acceleration and p-CMFD embedding of nonoverlapping local/global iterations, Nucl. Sci. Eng. (accepted for publication).

Yuk, S., Cho, B., Cho, N.Z., 2013. Comparison of non-overlapping and overlapping local/global iteration schemes for whole-core deterministic transport calculation. Trans. Kor. Nucl. Soc., Gyeongju, Korea, October 24–25, 2013, <http://www.kns.org/kns_files/kns/file/13F-02A-8A-%C0%B0%BD%C2%BC%F6.pdf>.